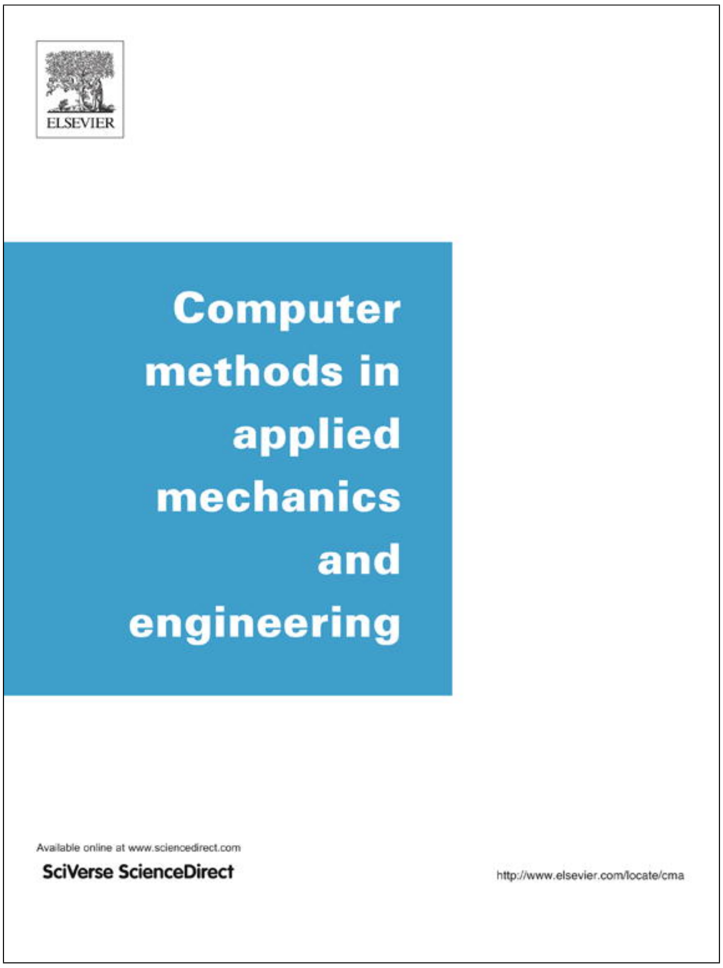

(This is a sample cover image for this issue. The actual cover is not yet available at this time.)

Comput. Methods Appl. Mech. Engrg. 247–248 (2012) 130–145

Contents lists available at SciVerse ScienceDirect

Comput. Methods Appl. Mech. Engrg.

journal homepage: www.elsevier.com/locate/cma

Evaluation of the stiffness tensor of a fractured medium with harmonic experiments

Juan E. Santos [a,b,c,*], Stefano Picotti [d], José M. Carcione [d]

[a] CONICET, Instituto del Gas y del Petróleo, Facultad de Ingeniería, Universidad de Buenos Aires, Av. Las Heras 2214 Piso 3 C1127AAR Buenos Aires, Argentina
[b] Universidad Nacional de La Plata, La Plata, Argentina
[c] Department of Mathematics, Purdue University, 150 N. University Street, West Lafayette, IN 47907-2067, USA
[d] Istituto Nazionale di Oceanografia e di Geofisica Sperimentale (OGS), Borgo Grotta Gigante 42c, 34010 Sgonico, Trieste, Italy

ARTICLE INFO

Article history:
Received 19 March 2012
Received in revised form 8 July 2012
Accepted 3 August 2012
Available online 24 August 2012

Keywords:
Fractured viscoelastic
Finite elements
Harmonic experiments
Anisotropy

ABSTRACT

A fractured medium behaves as an anisotropic medium when the wavelength is much larger than the distance between fractures. These are modeled as boundary discontinuities in the displacement and particle velocity. When the set of fractures is plane, the theory predicts that the equivalent medium is transversely isotropic and viscoelastic (TIV). We present a novel procedure to determine the complex and frequency-dependent stiffness components. The methodology amounts to perform numerical compressibility and shear harmonic tests on a representative sample of the medium. These tests are described by a collection of elliptic boundary-value problems formulated in the space-frequency domain, which are solved with a Galerkin finite-element procedure. The examples illustrate the implementation of the tests to determine the set of stiffnesses and the associated phase velocities and quality factors.

1. Introduction

Wave propagation through fractures is an important subject in seismology, exploration geophysics and mining (e.g. Schoenberg and Douma [1]). Modeling fractures requires an interface model for describing their dynamic response. Here, we consider that the stress components are proportional to the displacement and velocity discontinuities through the specific stiffnesses and viscosities, respectively. Displacement discontinuities conserve energy while velocity discontinuities generate energy loss at the interface. The specific viscosity accounts for the presence of a viscous liquid under saturated conditions, which introduces a viscous coupling between the two surfaces of the fracture [2–4].

A dense set of parallel plane fractures can be modeled as a TIV medium if the dominant wavelength of the traveling waves is much larger than the distance between the fractures. Chichinina et al. [5] described anisotropic attenuation in a TI medium using Schoenberg's linear-slip model with complex-valued normal and tangential fracture stiffnesses. Carcione et al. [6] generalized this theory by extending the orthorhombic model given in Schoenberg and Helbig [7] to the anelastic monoclinic case. The medium consists of sets of vertical fractures embedded in a TI background medium (generally horizontal fine layering) to form a long-wavelength equivalent monoclinic medium. There are a few papers presenting numerical approaches to determine effective media corresponding to fractured rocks. Grechka and Kachanov [8,9] perform 3D static finite-element simulations, summing up the individual contributions of the fractures and ignoring their interactions. An analysis of the non-interaction approximation and differential schemes to predict effective elastic properties of fractured media is presented in [10]. On the other hand, Saenger et al. [11] present a finite-difference procedure to solve the viscoelastic wave equation in the space–time domain. They apply a Heaviside source function and drive the system to the static limit, which yields the desired static stiffnesses coefficients. Besides, Saenger et al. [12] perform numerical simulations in 2D and 3D media saturated with fluids to analyze Biot's predictions in the high and low frequency limits of poroelasticity. An analysis on the effects of fracture heterogeneity, orientation and size on seismic signatures can be found in [13].

To test and validate Schoenberg's theory in [16], we present a novel finite element approach to determine the complex stiffness coefficients of the TIV equivalent medium [14]. The methodology consists of applying time-harmonic oscillatory tests at a finite number of frequencies. Each test is performed by using the viscoelastic wave equation of motion expressed in the space-frequency domain, with appropriate boundary conditions, and solved with a finite-element method (FEM). These tests can be regarded as an upscaling method to obtain the effect of the fine layering scale on the macroscale. Finally, we employ the finite element simulators to determine equivalent TIV effective media in more realistic scenarios for which no analytical solutions are available.

* Corresponding author at: Department of Mathematics, Purdue University, 150 N. University Street, West Lafayette, IN 47907-2067, USA. Tel.: +1 765 494 1925; fax: +1 765 494 0548.

E-mail address: santos@math.purdue.edu (J.E. Santos).

0045-7825/$ - see front matter © 2012 Elsevier B.V. All rights reserved.
http://dx.doi.org/10.1016/j.cma.2012.08.004

2. The stress–strain relations

Let us consider a viscoelastic background medium and its description in the frequency domain. The medium has a set of parallel (horizontal) fractures which are described by appropriate boundary conditions (see below). Let $\mathbf{x} = (x_1, x_2, x_3)$ and $u(\mathbf{x}) = (u_1, u_2, u_3)$ denote the time Fourier transform of the displacement vector of the viscoelastic medium. Let σ_{ij} and $e_{ij}(u)$ denote the stress and strain tensors of the medium. The stress–strain relations of a general anisotropic medium, including attenuation, are

$$\sigma_{jk}(u) = p_{jklm} e_{lm}(u), \quad e_{lm}(u) = \frac{1}{2}\left(\frac{\partial u_l}{\partial x_m} + \frac{\partial u_m}{\partial x_l}\right), \tag{1}$$

where the coefficients p_{jklm} are complex and frequency dependent [3].

When the background medium is isotropic and viscoelastic, the stress–strain relation is

$$\sigma_{jk}(u) = \lambda \delta_{jk} \nabla \cdot u + 2\mu e_{jk}(u), \tag{2}$$

where δ_{jk} is the Kroenecker delta and λ and μ are the complex Lamé constants.

Let $\rho = \rho(\mathbf{x})$ be the mass density. The equation of motion is

$$\omega^2 \rho u(\mathbf{x}, \omega) + \nabla \cdot \sigma(u(\mathbf{x}, \omega)) = 0, \tag{3}$$

where ω is the angular frequency, σ is given by (1) for a general medium and by (2) in the isotropic and viscoelastic case.

Let us consider x_1 and x_3 as the horizontal and vertical coordinates, respectively. If a dense set of parallel fractures is present, Schoenberg and Douma [1] have shown that the medium behaves as a TIV medium with a vertical x_3-axis of symmetry at long wavelengths. Denoting by τ_{ij} the stress tensor of the equivalent TIV medium at the macroscale, the corresponding stress–strain relations, stated in the space-frequency domain, are [15,3]

$$\tau_{11}(u) = p_{11}\epsilon_{11}(u) + p_{12}\epsilon_{22}(u) + p_{13}\epsilon_{33}(u), \tag{4}$$
$$\tau_{22}(u) = p_{12}\epsilon_{11}(u) + p_{11}\epsilon_{22}(u) + p_{13}\epsilon_{33}(u), \tag{5}$$
$$\tau_{33}(u) = p_{13}\epsilon_{11}(u) + p_{13}\epsilon_{22}(u) + p_{33}\epsilon_{33}(u), \tag{6}$$
$$\tau_{23}(u) = 2p_{55}\epsilon_{23}(u), \tag{7}$$
$$\tau_{13}(u) = 2p_{55}\epsilon_{13}(u), \tag{8}$$
$$\tau_{12}(u) = 2p_{66}\epsilon_{12}(u). \tag{9}$$

Schoenberg's theory predicts that if the background medium is homogeneous, the stiffnesses p_{IJ}'s in (4)–(9) are given by [16,6]

$$p_{11} = p_{22} = E - \lambda^2 Z_N c_N, \quad p_{12} = \lambda - \lambda^2 Z_N c_N \quad p_{13} = \lambda c_N, \tag{10}$$
$$p_{33} = E c_N, \quad p_{55} = \mu c_T, \quad p_{66} = \mu.$$

where

$$c_N = (1 + E Z_N)^{-1} \quad \text{and} \quad c_T = (1 + \mu Z_T)^{-1}, \tag{11}$$

Z_N and Z_T are the normal and tangential complex compliances of the fractures (see below) and $E = \lambda + 2\mu$. The theory assumes that distance between fractures is much smaller than the wavelength of the signal and that the boundary condition is the same for all the fractures. Moreover, we assume that the fracture distance is constant, i.e., there is periodicity. On the other hand, the numerical solver may consider an inhomogeneous background medium, unequal fracture distances and dissimilar boundary conditions at the fractures surfaces.

Remark. The ϵ_{ij}'s are strain components at the macroscale.

The p_{IJ} are the complex and frequency-dependent Voigt stiffnesses to be determined numerically with the harmonic experiments and compared to those given in Eq. (10). In the next section, we present a numerical procedure to determine the coefficients in (4)–(9) and the corresponding phase velocities and quality factors. We will show that for this purpose it is sufficient to perform a collection of oscillatory tests on representative 2D samples of the viscoelastic material.

3. Determination of the stiffness components

In order to determine the coefficients in (4)–(9) we proceed as follows. We solve (3) in the 2D case on a reference square $\Omega = (0, H)^2$ with boundary Γ in the (x_1, x_3)-plane.

Set $\Gamma = \Gamma^L \cup \Gamma^B \cup \Gamma^R \cup \Gamma^T$, where

$$\Gamma^L = \{(x_1, x_3) \in \Gamma : x_1 = 0\}, \quad \Gamma^R = \{(x_1, x_3) \in \Gamma : x_1 = H\},$$
$$\Gamma^B = \{(x_1, x_3) \in \Gamma : x_3 = 0\}, \quad \Gamma^T = \{(x_1, x_3) \in \Gamma : x_3 = H\}.$$

Denote by ν the unit outer normal on Γ and let χ be a unit tangent on Γ so that $\{\nu, \chi\}$ is an orthonormal system on Γ.

Let us assume that we have a set of $J^{(f)}$ horizontal fractures $\Gamma^{(f,l)}, \ l = 1, \ldots, J^{(f)}$ each one of length L in our domain Ω. This set of fractures divides our domain in a collection of nonoverlapping rectangles $R^{(l)}, \ l = 1, \ldots, J^f + 1$, so that

$$\Omega = \cup_{l=1}^{J^{(f)}+1} R^{(l)}.$$

Consider a fracture $\Gamma^{(f,t)}$ and the two rectangles $R^{(t)}$ and $R^{(t+1)}$ having as a common side $\Gamma^{(f,t)}$. Let $\nu_{t,t+1}, \chi_{t,t+1}$ be the unit outer normal and a unit tangent (oriented counterclockwise) on $\Gamma^{(f,t)}$ from $R^{(t)}$ to $R^{(t+1)}$, such that $\{\nu_{t,t+1}, \chi_{t,t+1}\}$ are an orthonormal system on $\Gamma^{(f,t)}$.

The boundary conditions at each one of the fractures $\Gamma^{(f,t)}$ are the stress continuity and the condition that stress components be proportional to the displacement and velocity discontinuities through specific stiffnesses and viscosities, respectively. More precisely, if $u^{(t)} = u|_{R^{(t)}}$ denotes the restriction of u_i to $R^{(t)}$, we will impose the conditions

$$\sigma(u^{(t)})\nu_{t,t+1} = \sigma(u^{(t+1)})\nu_{t,t+1} \quad (x_1, x_3) \in \Gamma^{(f,t)}, \quad t = 1, \ldots, J^{(f)}, \tag{12}$$

$$\left(\sigma(u^{(t)})\nu_{t,t+1} \cdot \nu_{t,t+1}, \sigma(u^{(t)})\nu_{t,t+1} \cdot \chi_{t,t+1}\right)^T$$
$$= \mathbf{D}^{(t)}(\omega)\left([u] \cdot \nu_{t,t+1}, [u] \cdot \chi_{t,t+1}\right)^T \quad (x_1, x_3) \in \Gamma^{(f,t)}, \quad t = 1, \ldots, J^{(f)}. \tag{13}$$

where T indicates the transpose, $[u]$ denotes the jump at $\Gamma^{(f,t)}$ of displacement vector u, i.e.,

$$[u] = (u^{(t)} - u^{(t+1)})|_{\Gamma^{(f,t)}}$$

and

$$\mathbf{D}^{(t)}(\omega) = \begin{pmatrix} \alpha^{(t)} & 0 \\ 0 & \beta^{(t)} \end{pmatrix} \tag{14}$$

where

$$\alpha^{(t)}(x_1, x_3, \omega) = \alpha_R^{(t)}(x_1, x_3) + i\omega \alpha_I^{(t)}(x_1, x_3) \tag{15}$$
$$\beta^{(t)}(x_1, x_3, \omega) = \beta_R^{(t)}(x_1, x_3) + i\omega \beta_I^{(t)}(x_1, x_3), \quad t = 1, \ldots, J^{(f)},$$

are the complex (scalar) stiffnesses (per unit length, i.e., stress/length) associated with the fractures. It will be assumed that $\alpha_R^{(t)}, \alpha_I^{(t)}, \beta_R^{(t)}$ and $\beta_I^{(t)}$ are strictly positive. These stiffnesses and the compliances in Eq. (10) and (11) are related as

$$L Z_N^{(t)} \alpha^{(t)} = 1 \quad \text{and} \quad L Z_T^{(t)} \beta^{(t)} = 1, \tag{16}$$

where L is the average spacing between the fractures.

Let us omit the superscript (t) for simplicity in the following. The components (10) can be obtained by assuming a periodic medium composed of two layers, where one of the layers has the Lamé constants λ and μ (the background medium) and the other, representing the fracture, is very thin with Lamé constants $\mu_f = pL\beta = p/Z_T$ and $E_f = \lambda_f + 2\mu_f = pL\alpha = p/Z_N$, where $p \ll 1$ is the volume proportion of fractures, and L is the fracture spacing (constant). The displacement discontinuities (boundary conditions) associated with the fractures are $[u]_3 = LZ_N\sigma_{33}$ and $[u]_1 = LZ_T\sigma_{13}$ along the x_3 – and x_1-directions, respectively (see Schoenberg [16], Eqs. (21)–(23).

According to Eq. (16), the imaginary parts of $Z_N^{(t)}$ and $Z_T^{(t)}$ are negative, since $\alpha_R^{(t)}, \alpha_I^{(t)}, \beta_R^{(t)}$ and $\beta_I^{(t)}$ are defined strictly positive.

The compliances Z (Z_N or Z_T) are complex and frequency-dependent and can be expressed as [4,6]

$$Z^{-1} = L(\kappa + i\omega\eta), \tag{17}$$

where κ is a specific stiffness and η is a specific viscosity, having dimensions of stiffness and viscosity per unit length, respectively.

It follows how to obtain the stiffness components.

(i) To determine p_{33}, we solve (3) in Ω using the fracture boundary conditions (12) and (13) and the following boundary conditions:

$$\sigma(u)\nu\cdot\nu = -\Delta P, \quad (x_1,x_3)\in\Gamma^T, \tag{18}$$
$$\sigma(u)\nu\cdot\chi = 0, \quad (x_1,x_3)\in\Gamma, \tag{19}$$
$$u\cdot\nu = 0, \quad (x_1,x_3)\in\Gamma^L\cup\Gamma^R\cup\Gamma^B. \tag{20}$$

In this experiment $\epsilon_{11}(u) = \epsilon_{22}(u) = 0$ and from (6) we see that this experiment determines p_{33} as follows.

Denoting by V the original volume of the sample, its (complex) oscillatory volume change, $\Delta V(\omega)$, we note that

$$\frac{\Delta V(\omega)}{V} = -\frac{\Delta P}{p_{33}(\omega)}, \tag{21}$$

valid in the quasistatic case.

After solving (3) with the boundary conditions (12) and (13) and (18)–(20), the vertical displacements $u_3(x,H,\omega)$ on Γ^T allow us to obtain an average vertical displacement $u_3^{s,T}(\omega)$ suffered by the boundary Γ^T. Then, for each frequency ω, the volume change produced by the compressibility test can be approximated by $\Delta V(\omega)\approx Hu_3^{s,T}(\omega)$, which enable us to compute $p_{33}(\omega)$ by using the relation (21).

(ii) To determine p_{11}, we solve (3) in Ω using (12) and (13) plus the following boundary conditions

$$\sigma(u)\nu\cdot\nu = -\Delta P, \quad (x_1,x_3)\in\Gamma^R, \tag{22}$$
$$\sigma(u)\nu\cdot\chi = 0, \quad (x_1,x_3)\in\Gamma, \tag{23}$$
$$u\cdot\nu = 0, \quad (x_1,x_3)\in\Gamma^L\cup\Gamma^B\cup\Gamma^T. \tag{24}$$

In this experiment $\epsilon_{33}(u) = \epsilon_{22}(u) = 0$ and from (4) we see that this experiment determines p_{11} as indicated for p_{33} measuring the oscillatory volume change.

(iii) To determine p_{55}, let us consider the solution of (3) in Ω with the fracture boundary conditions (12) and (13) added to the following boundary conditions

$$-\sigma(u)\nu = g, \quad (x_1,x_3)\in\Gamma^T\cup\Gamma^L\cup\Gamma^R, \tag{25}$$
$$u = 0, \quad (x_1,x_3)\in\Gamma^B, \tag{26}$$

where

$$g = \begin{cases} (0,\Delta G), & (x_1,x_3)\in\Gamma^L, \\ (0,-\Delta G), & (x_1,x_3)\in\Gamma^R, \\ (-\Delta G,0), & (x_1,x_3)\in\Gamma^T. \end{cases}$$

The change in shape of the rock sample allows to recover $p_{55}(\omega)$ by using the relation

$$tg(\theta(\omega)) = \frac{\Delta G}{p_{55}(\omega)}, \tag{27}$$

where $\theta(\omega)$ is the departure angle between the original positions of the lateral boundaries and those after applying the shear stresses (see for example, [17]).

Measuring the horizontal displacements $u_1(x_1,H,\omega)$ at the top boundary Γ^T, we obtain an average horizontal displacement $u_1^{s,T}(\omega)$ suffered by the boundary Γ^T. This average value allows us to approximate the change in shape by $tg(\theta(\omega))\approx u_1^{s,T}(\omega)/H$, which from (27) let us estimate $p_{55}(\omega)$.

(iv) The stiffness p_{66} is associated with shear waves traveling in the (x_1,x_2)-plane. We consider a fractured horizontal slab in the x_2-direction and an homogeneous sample $\Omega_2 = (0,H)^2$ in the (x_1,x_2)-plane, with boundary $\Gamma_2 = \Gamma_2^L\cup\Gamma_2^B\cup\Gamma_2^R\cup\Gamma_2^T$, where

$$\Gamma_2^L = \{(x_1,x_2)\in\Gamma : x_1 = 0\}, \quad \Gamma_2^R = \{(x_1,x_2)\in\Gamma : x_1 = H\},$$
$$\Gamma_2^B = \{(x_1,x_2)\in\Gamma : x_2 = 0\}, \quad \Gamma^T = \{(x_1,x_2)\in\Gamma : x_2 = H\}.$$

We then consider the solution of (3) in Ω_2 using the conditions (12) and (13) added to the following boundary conditions

$$-\sigma(u)\nu = g, \quad (x_1,x_3)\in\Gamma_2^T\cup\Gamma_2^L\cup\Gamma_2^R, \tag{28}$$
$$u = 0, \quad (x_1,x_2)\in\Gamma_2^B, \tag{29}$$

where

$$g = \begin{cases} (0,\Delta G), & (x_1,x_2)\in\Gamma_2^L, \\ (0,-\Delta G), & (x_1,x_2)\in\Gamma_2^R, \\ (-\Delta G,0), & (x_1,x_2)\in\Gamma_2^T. \end{cases}$$

Thus, we proceed as indicated for $p_{55}(\omega)$.

The calculation of p_{66} requires an alternative treatment due to the fact that the sample is finite along the fracture planes which do not remain parallel after the deformation. In this case, we set to zero the displacement perpendicular to those planes. This constraint has no effect on the calculation since this component is uncoupled from the motion related to p_{66}.

(v) To determine p_{13} we solve (3) in Ω using (12) and (13) with the additional boundary conditions

$$\sigma(u)\nu\cdot\nu = -\Delta P, \quad (x_1,x_3)\in\Gamma^R\cup\Gamma^T, \tag{30}$$
$$\sigma(u)\nu\cdot\chi = 0, \quad (x_1,x_3)\in\Gamma, \tag{31}$$
$$u\cdot\nu = 0, \quad (x_1,x_3)\in\Gamma^L\cup\Gamma^B. \tag{32}$$

Thus, in this experiment $\epsilon_{22} = 0$, and from (4) and (6) we get

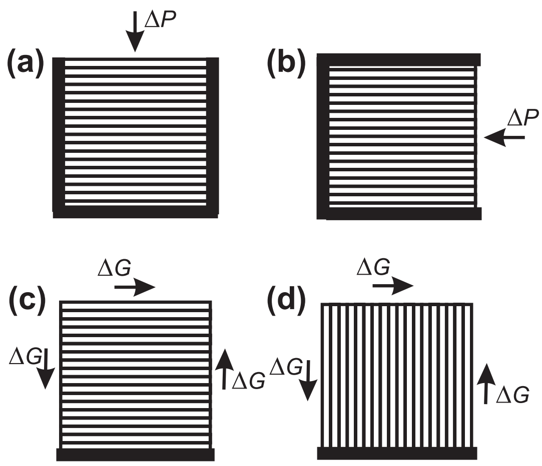

Fig. 1. Harmonic tests performed to obtain (a) p_{33}, (b) p_{11} (c) p_{55} and (d) p_{66} The orientation of the horizontal fractures and the directions of the applied stresses on the boundaries are indicated. The thick black lines indicate zero normal displacements in (a) and (b) and zero displacements in (c) and (d) as in (20), (24), (26) and (29).

$$\tau_{11} = p_{11}\epsilon_{11} + p_{13}\epsilon_{33},$$
$$\tau_{33} = p_{13}\epsilon_{11} + p_{33}\epsilon_{33}, \tag{33}$$

where ϵ_{11} and ϵ_{33} are the (macroscopic) strain components at the right lateral side and top side of the sample, respectively. Then from (33) and the fact that $\tau_{11} = \tau_{33} = -\Delta P$ (c.f. (30)) we obtain $p_{13}(\omega)$ as

$$p_{13}(\omega) = \frac{p_{11}\epsilon_{11} - p_{33}\epsilon_{33}}{\epsilon_{11} - \epsilon_{33}}. \tag{34}$$

Figs. 1(a)–(d) illustrate the experiments needed to compute the stiffnesses components.

4. The variational formulation

To state a variational formulation for the boundary-value problems defined in the previous section we need to introduce some notation. For $X \subset \mathbb{R}^d$ with boundary ∂X, let $(\cdot,\cdot)_X$ and $\langle\cdot,\cdot\rangle_{\partial X}$ denote the complex $L^2(X)$ and $L^2(\partial X)$ inner products for scalar, vector, or matrix valued functions. Also, for $s \in \mathbb{R}$, $\|\cdot\|_{s,X}$ will denote the usual norm for the Sobolev space $H^s(X)$ [18]. In addition, if $X = \Omega$ or $X = \Gamma$, the subscript X may be omitted such that $(\cdot,\cdot) = (\cdot,\cdot)_\Omega$ or $\langle\cdot,\cdot\rangle = \langle\cdot,\cdot\rangle_\Gamma$. Also, let us introduce the following closed subspaces of $[H^1(\Omega)]^2$ and $[H^1(\Omega_2)]^2$:

$$\mathcal{W}_{11}(\Omega) = \{v \in [L^2(\Omega)]^2 : v|_{R^{(l)}} \in [H^1(R^{(l)})]^2,\ v\cdot\nu = 0 \text{ on } \Gamma^B \cup \Gamma^T \cup \Gamma^L\},$$

$$\mathcal{W}_{33}(\Omega) = \{v \in [L^2(\Omega)]^2 : v|_{R^{(l)}} \in [H^1(R^{(l)})]^2,\ v\cdot\nu = 0 \text{ on } \Gamma^L \cup \Gamma^R \cup \Gamma^B\},$$

$$\mathcal{W}_{13}(\Omega) = \{v \in [L^2(\Omega)]^2 : v|_{R^{(l)}} \in [H^1(R^{(l)})]^2,\ v\cdot\nu = 0 \text{ on } \Gamma^L \cup \Gamma^B\},$$

$$\mathcal{W}_{55}(\Omega) = \{v \in [L^2(\Omega)]^2 : v|_{R^{(l)}} \in [H^1(R^{(l)})]^2,\ v = 0 \text{ on } \Gamma^B\},$$

$$\mathcal{W}_{66}(\Omega_2) = \{v \in [L^2(\Omega_2)]^2 :: v|_{R^{(l)}} \in [H^1(R^{(l)})]^2,\ v = 0 \text{ on } \Gamma_2^B\}.$$

Set

$$\Lambda(u,v) = -\omega^2(u,v) + \sum_{l=1}^{J^{(f)}+1}\sum_{s,t=1,3}(\sigma_{st}(u),\epsilon_{st}(v))_{R^{(l)}} + \sum_{l=1}^{J^{(f)}}\left[\left\langle\alpha^{(l)}[u]_3,[v]_3\right\rangle_{\Gamma^{(f,l)}} + \left\langle\beta^{(l)}[u]_1,[v]_1\right\rangle_{\Gamma^{(f,l)}}\right]. \tag{35}$$

Note that the term $\sum_{l=1}^{J^{(f)}+1}\sum_{s,t=1,3}(\sigma_{st}(u),\epsilon_{st}(v))_{R^{(l)}}$ in (35) can be written in the form

$$\sum_{l=1}^{J^{(f)}+1}\sum_{s,t=1,3}(\sigma_{st}(u),\epsilon_{st}(v))_{R^{(l)}} = \sum_{l=1}^{J^{(f)}+1}(\mathbf{M}(\omega)\tilde\epsilon(u),\tilde\epsilon(v))_{R^{(l)}} = \sum_{l=1}^{J^{(f)}+1}(\mathbf{M}_R(\omega)\tilde\epsilon(u),\tilde\epsilon(v))_{R^{(l)}} + i(\mathbf{M}_I(\omega)\tilde\epsilon(u),\tilde\epsilon(v))_{R^{(l)}}, \tag{36}$$

where $\mathbf{M}(\omega) = \mathbf{M}_R(\omega) + i\mathbf{M}_I(\omega)$ is a complex matrix given by

$$\mathbf{M}(\omega) = \begin{pmatrix} \lambda(\omega)+2\mu(\omega) & \lambda(\omega) & 0 \\ \lambda(\omega) & \lambda(\omega)+2\mu(\omega) & 0 \\ 0 & 0 & 4\mu(\omega) \end{pmatrix}. \tag{37}$$

and

$$\tilde\epsilon(u) = \begin{pmatrix} \epsilon_{11}(u) \\ \epsilon_{33}(u) \\ \epsilon_{13}(u) \end{pmatrix}.$$

It will be assumed that the real part $\mathbf{M}_R(\omega)$ is positive definite since in the elastic limit it is associated with the strain energy density. Furthermore, the imaginary parts $\mathbf{M}_I(\omega)$ are assumed to be positive definite because of the restriction imposed on our system by the first and second laws of thermodynamics. See [19] and the appendix in [20] for a proof of the validity of these assumptions.

Furthermore, note that

$$\begin{aligned}\Lambda(u,u) = {}& -\omega^2(\rho u,u) + \sum_{l=1}^{J^{(f)}+1}(\mathbf{M}_R\tilde\epsilon(u),\tilde\epsilon(u))_{R^{(l)}} + \sum_{l=1}^{J^{(f)}}\left\langle\alpha_R^{(l)}[u]_3,[u]_3\right\rangle_{\Gamma^{(f,l)}} \\ & + \left\langle\beta_R^{(l)}[u]_1,[u]_1\right\rangle_{\Gamma^{(f,l)}} + i\left[\sum_{l=1}^{J^{(f)}+1}(\mathbf{M}_I\tilde\epsilon(u),\tilde\epsilon(u))_{R^{(l)}}\right. \\ & \left. +\omega\sum_{l=1}^{J^{(f)}}\left\langle\alpha_I^{(l)}[u]_3,[u]_3\right\rangle_{\Gamma^{(f,l)}} + \left\langle\beta_I^{(l)}[u]_1,[u]_1\right\rangle_{\Gamma^{(f,l)}}\right] \\ \equiv {}& \mathrm{Re}(\Lambda(u,u)) + i\mathrm{Im}(\Lambda(u,u)).\end{aligned} \tag{38}$$

Thus, since the matrices $\mathbf{M}_R$ and $\mathbf{M}_I$ are positive definite and the stiffnesses coefficients $\alpha_R^{(l)}, \alpha_I^{(l)}, \beta_R^{(l)}$ and $\beta_I^{(l)}$ are positive, for each frequency ω we may associate $\mathrm{Re}(\Lambda(u,u))$ and $\mathrm{Im}(\Lambda(u,u))$ with the Fourier transform of the strain energy of our fractured viscoelastic medium evaluated at that frequency. The imaginary part $\mathrm{Im}(\Lambda(u,u))$ takes into account the energy losses due to both the viscoelastic character of the material and the dissipative effect of the fractures.

Next, multiply equation (3) by $v \in \mathcal{W}_{33}(\Omega)$, use integration by parts and apply the boundary conditions (12), (13) and (18)–(20) to obtain the following variational formulation associated with the coefficient $p_{33}(\omega)$: find $u^{(33)} \in \mathcal{W}_{33}(\Omega)$ such that:

$$\Lambda(u^{(33)},v) = -\langle\Delta P, v\cdot\nu\rangle_{\Gamma^T}, \quad \forall v \in \mathcal{W}_{33}(\Omega). \tag{39}$$

Proceeding similarly, we obtain the following weak formulations for the other p_{IJ}'s coefficients:

For p_{11}: find $u^{(11)} \in \mathcal{W}_{11}(\Omega)$ such that:

$$\Lambda(u^{(11)},v) = -\langle\Delta P, v\cdot\nu\rangle_{\Gamma^R}, \quad \forall v \in \mathcal{W}_{11}(\Omega). \tag{40}$$

For p_{13}: find $u^{(13)} \in \mathcal{W}_{13}(\Omega)$ such that:

$$\Lambda(u^{(13)},v) = -\langle\Delta P, v\cdot\nu\rangle_{\Gamma^R\cup\Gamma^T}, \quad \forall v \in \mathcal{W}_{13}(\Omega). \tag{41}$$

For p_{55}: find $u^{(55)} \in \mathcal{W}_{55}(\Omega)$ such that:

$$\Lambda(u^{(55)},v) = -\langle g, v\rangle_{\Gamma\setminus\Gamma^B}, \quad \forall v \in \mathcal{W}_{55}(\Omega). \tag{42}$$

For p_{66}: find $u^{(66)} \in \mathcal{W}_{66}(\Omega)$ such that:

$$\Lambda(u^{(66)},v) = -\langle g, v\rangle_{\Gamma_2\setminus\Gamma_2^B}, \quad \forall v \in \mathcal{W}_{66}(\Omega). \tag{43}$$

The above formulated boundary-value problems (BVP's) are associated with non-coercive second-order elliptic operators having boundary data in $L^2(\Omega)$, and their solutions are discontinuous across the fractures $\Gamma^{(f,l)}$, $l = 1,\dots,J^{(f)}$. Consequently, their solutions will be assumed to belong locally to $[H^{3/2}]^2$, i.e., we will assume that $u^{(t)} \in [H^{3/2}(R^{(t)})]^2$, $t = 1,\dots,J^{(f)}+1$ [21]. This maximal regularity will be used to analyze the well-posedeness of our BVP's and to derive our error estimates.

To analyze the uniqueness of the solution of (39), set $\Delta P = 0$ and choose $v = u^{(33)}$ in (39) to obtain the equation

$$\begin{aligned}& -\omega^2(\rho u^{(33)},u^{(33)}) + \sum_{l=1}^{J^{(f)}+1}(\mathbf{M}_R\tilde\epsilon(u^{(33)}),\tilde\epsilon(u^{(33)}))_{R^{(l)}} + i\sum_{l=1}^{J^{(f)}+1}(\mathbf{M}_I\tilde\epsilon(u^{(33)}), \\ & \tilde\epsilon(u^{(33)}))_{R^{(l)}} + \sum_{l=1}^{J^{(f)}}\left[\left\langle(\alpha_R^{(l)}+i\omega\alpha_I^{(l)})[u^{(33)}]_3,[u^{(33)}]_3\right\rangle_{\Gamma^{(f,l)}}\right. \\ & \left. +\left\langle(\beta_R^{(l)}+i\omega\beta_I^{(l)})[u^{(33)}]_1,[u^{(33)}]_1\right\rangle_{\Gamma^{(f,l)}}\right] = 0.\end{aligned} \tag{44}$$

Taking the imaginary part in (44) and using that $\mathbf{M}_I$ is positive definite and that $\alpha_I > 0,\ \beta_I > 0$ we conclude that

$$\epsilon_{11}(u^{(33)}) = 0, \quad \text{in} \quad L^2(R^{(l)}), \tag{45}$$

$$\epsilon_{33}(u^{(33)}) = 0, \quad \text{in} \quad L^2(R^{(l)}), \tag{46}$$

$$\epsilon_{13}(u^{(33)}) = 0, \quad \text{in} \quad L^2(R^{(l)}). \tag{47}$$

$$\epsilon_{11}(u^{(33)}) = \frac{\partial u_1^{(13)}(x_1,x_3)}{\partial x_1} = 0, \quad \epsilon_{33}(u^{(3)}) = \frac{\partial u_3^{(13)}(x_1,x_3)}{\partial x_3} = 0, \quad \text{a.e.} \quad \text{in } R^{(l)},$$

so that

$$u_1^{(33)}(x_1,x_3) = f^{(l)}(x_3), \quad u_3^{(33)}(x_1,x_3) = g^{(l)}(x_1) \quad \text{a.e.} \quad \text{in} \quad L^2(R^{(l)}). \tag{48}$$

Thus from (47) and (48) have

$$2\epsilon_{13}(u^{(13)}) = \frac{\partial f^{(l)}(x_3)}{\partial x_3} + \frac{\partial g^{(l)}(x_1)}{\partial x_1} = 0, \quad \text{a.e.} \quad \text{in} \quad R^{(l)}, \tag{49}$$

which in turn implies

$$\frac{\partial f^{(l)}(x_3)}{\partial x_3} = -\frac{\partial g^{(l)}(x_1)}{\partial x_1} = C^{(l)} = \text{constant} \quad \text{a.e.} \quad \text{in} \quad R^{(l)}. \tag{50}$$

Hence,

$$g^{(l)}(x_1) = -C^{(l)}x_1 + A^{(l)}, \quad f(l)(x_3) = C^{(l)}x_3 + B^{(l)}, \quad \text{a.e.} \quad \text{in} \quad R^{(l)}. \tag{51}$$

Next, by the Sobolev embedding theorem [18]

$$H^{3/2}(R^{(l)}) \to C^0(\overline{R}^{(l)}), \tag{52}$$

so that $u_1^{(33)}, u_3^{(33)}$ are uniformly continuous functions on $R^{(l)}$. Consequently (48) holds for all $(x_1,x_3) \in \overline{R}^{(l)}$ as uniformly continuous functions, and $u_1^{(33)}, u_3^{(33)}$ have unique extensions to $\partial R^{(l)}$. Hence,

$$u_1^{(33)}(x_1,x_3) = f^{(l)}(x_3), \quad u_3^{(33)}(x_1,x_3) = g^{(l)}(x_1) \quad \forall \quad (x_1,x_3) \in \overline{R}^{(l)}. \tag{53}$$

On the other hand, the boundary condition (20) tells us that the normal components of the traces of $u^{(33)}$ vanish on $\Gamma^B \cup \Gamma^L$, so that

$$u_1^{(33)}(0,x_3) = 0, \quad u_3^{(33)}(x_1,0) = 0. \tag{54}$$

Thus (53) and (54) imply that

$$u_1^{(33)}(x_1,x_3) = u_3^{(33)}(x_1,x_3) = 0. \tag{55}$$

and we have uniqueness for the solution of (39). Uniqueness for the solution of (40) and (41) follows with the same argument.

Let us turn to analyze the uniqueness of the solution of (42). Set $g = 0$ choose $v = u^{(55)}$ in (42). Choosing the imaginary part in the resulting equation, we obtain

$$\tilde{\epsilon}(u^{(55)}) = 0, \quad \text{in} \quad L^2(R^{(l)}). \tag{56}$$

Next, recall Korn's second inequality [22]:

$$\sum_{l,m=1,3} \|\epsilon_{lm}(v)\|^2_{R^{(l)}} + \|v\|_0^2 \geqslant C_1\|v\|^2_{1,R^{(l)}}, \quad \forall \quad v \in [H^1(R(l))]^2, \tag{57}$$

and that for any $v \in [H^1(R^{(l)})]^2$ vanishing on a subset of positive measure of $\partial R^{(l)}$, using (57) it can be shown that [23]

$$|||v||| = \left(\sum_{s,t=1,3} \|\epsilon_{st}(v)\|^2_{0,R^{(l)}}\right)^{1/2} \tag{58}$$

defines a norm for v equivalent to the H^1-norm. Thus, for some positive constants C_2, C_3,

$$C_2\|v\|_{1,R^{(l)}} \leqslant |||v||| \leqslant C_3\|v\|_{1R^{(l)}}, \quad \forall v \in \mathcal{W}_{55}(\Omega). \tag{59}$$

Consequently, (56) and (59) imply that

$$\|u^{(55)}\|_{1,R^{(l)}} = 0 \tag{60}$$

and we have uniqueness for the solution of (42).

5. The finite element method

Let $\mathcal{T}^h(\Omega)$ be a non-overlapping partition of Ω into rectangles Ω_j of diameter bounded by h such that $\overline{\Omega} = \cup_{j=1}^J \overline{\Omega}_j$. We will assume the Ω_j's are such that their horizontal sides either have empty intersection with the fractures or they coincide with one of the fractures.

Let

$$\Omega^f = \cup_{j=1}^{I_f} \Omega_j$$

where I_f is the number of Ω_j's having one top or bottom side contained in some fracture $\Gamma^{(f,l)}$ for some l in the range $1 \leqslant l \leqslant J^{(f)}$.

Set

$$\Omega^{Nf} = \Omega \setminus \Omega^f = \cup_{j=1}^{I_{Nf}} \Omega_j$$

where I_{Nf} is the number of all Ω_j's such that $\partial\Omega_j \cap \Gamma^{f,l} = \emptyset \forall l$.

Let

$$\mathcal{N}_j^h = P_{1,1}(\Omega_j) \times P_{1,1}(\Omega_j)$$

be two copies of the bilinear polynomials on Ω_j.

Denote by $\Gamma_{jk} = \partial\Omega_j \cap \partial\Omega_k$ the common side of two adjacent rectangles Ω_j and Ω_k and set

$$\mathcal{W}_{33}^{h,Nf}(\Omega^{Nf}) = \{v : v|_{\Omega_j} \in \mathcal{N}_j^h, v \text{ is continuous across } \Gamma_{jk} \text{ for all } \Omega_j \subset \Omega^{Nf}, \Omega_k \subset \Omega^{Nf}, v \cdot \nu = 0 \text{ on } \Gamma \setminus \Gamma^T\}$$

and

$$\mathcal{W}_{33}^{h,f}(\Omega^f) = \{v : v|_{\Omega_j} \in \mathcal{N}_j^h, \text{ for all } \Omega_j \subset \Omega^f, v \cdot \nu = 0 \text{ on } \Gamma \setminus \Gamma^T\}.$$

To determine p_{33} we will employ the following finite element space:

$$\mathcal{W}_{33}^h(\Omega) = \mathcal{W}_{33}^{h,N_f}(\Omega^{N_f}) \cup \mathcal{W}_{33}^{h,f}(\Omega^f). \tag{61}$$

Similarly, for p_{11} and p_{13} we define

$$\mathcal{W}_{11}^{h,Nf}(\Omega^{Nf}) = \{v : v|_{\Omega_j} \in \mathcal{N}_j^h, v \text{ is continuous across } \Gamma_{jk} \text{ for all } \Omega_j \subset \Omega^{Nf}, \Omega_k \subset \Omega^{Nf}, \ v \cdot \nu = 0 \text{ on } \Gamma \setminus \Gamma^R\},$$

$$\mathcal{W}_{11}^{h,f}(\Omega^f) = \{v : v|_{\Omega_j} \in \mathcal{N}_j^h, \ \forall\ \Omega_j \subset \Omega^f, v \cdot \nu = 0 \text{ on } \Gamma \setminus \Gamma^R\},$$

$$\mathcal{W}_{13}^{h,Nf}(\Omega^{Nf}) = \{v : v|_{\Omega_j} \in \mathcal{N}_j^h, v \text{ is continuous across } \Gamma_{jk} \text{ for all } \Omega_j \subset \Omega^{Nf}, \Omega_k \subset \Omega^{Nf}, \ v \cdot \nu = 0 \text{ on } \Gamma^L \cup \Gamma^B\}.$$

$$\mathcal{W}_{13}^{h,f}(\Omega^f) = \{v : v|_{\Omega_j} \in \mathcal{N}_j^h, \text{ for all } \Omega_j \subset \Omega^f, v \cdot \nu = 0 \text{ on } \Gamma^L \cup \Gamma^B\}.$$

Then to determine p_{11} we will employ the space

$$\mathcal{W}_{11}^h(\Omega) = \mathcal{W}_{11}^{h,N_f}(\Omega^{N_f}) \cup \mathcal{W}_{11}^{h,f}(\Omega^f). \tag{62}$$

while for p_{13} we will use

$$\mathcal{W}_{13}^h(\Omega) = \mathcal{W}_{13}^{h,N_f}(\Omega^{N_f}) \cup \mathcal{W}_{13}^{h,f}(\Omega^f). \tag{63}$$

Next, for the coefficient p_{55} let us introduce the sets

$$\mathcal{W}_{55}^{h,Nf}(\Omega^{Nf}) = \{v : v|_{\Omega_j} \in \mathcal{N}_j^h, v \text{ is continuous across } \Gamma_{jk} \text{ for all } \Omega_j \subset \Omega^{Nf}, \Omega_k \subset \Omega^{Nf}\ \ v = 0 \text{ on } \Gamma^B\},$$

$$\mathcal{W}_{55}^{h,f}(\Omega^f) = \{v : v|_{\Omega_j} \in \mathcal{N}_j^h, \text{ for all } \Omega_j \subset \Omega^f, v = 0 \text{ on } \Gamma^B\}.$$

To determine p_{55} we will employ the space

$$\mathcal{W}_{55}^h(\Omega) = \mathcal{W}_{55}^{h,N_f}(\Omega^{N_f}) \cup \mathcal{W}_{55}^{h,f}(\Omega^f). \tag{64}$$

Finally, for p_{66} we define

$$\Omega_2^f = \cup_{j=1}^{I_{2f}} \Omega_{2,j}$$

where $I_{2,f}$ is the number of rectangles $\Omega_{2,j}j$ of the partition of Ω_2 having one top or bottom side contained in some fracture $\Gamma_2^{(f,l)}$ for some l in the range $1 \leqslant l \leqslant J_2^{(f)}$ and set

$$\Omega_2^{Nf} = \Omega_2 \setminus \Omega_2^f \cup_{j=1}^{I_{Nf2}} \Omega_{2,j}$$

where I_{Nf2} is the number of all $\Omega_{2,j}$'s such that $\partial\Omega_{2,j} \cap \Gamma_2^{f,l} = \emptyset \forall l$. Then we define

$$\mathcal{W}_{66}^{h,Nf}(\Omega_2^{Nf}) = \{v : v|_{\Omega_{2,j}} \in \mathcal{N}_j^h, v \text{ is continuous across } \Gamma_{jk} \text{ for all } \Omega_{2,j} \subset \Omega^{Nf2}, \Omega_{2,k} \subset \Omega_2^{Nf},\ \ v = 0 \text{ on } \Gamma_2^B\},$$

$$\mathcal{W}_{66}^{h,f}(\Omega_2^f) = \{v : v|_{\Omega_j} \in \mathcal{N}_j^h, \text{ for all } \Omega_{2,j} \subset \Omega_2^f, v = 0 \text{ on } \Gamma_2^B\},$$

and to determine p_{66} we use the space

$$\mathcal{W}_{66}^h(\Omega_2) = \mathcal{W}_{66}^{h,N_f}(\Omega_2^{N_f}) \cup \mathcal{W}_{66}^{h,f}(\Omega_2^f). \tag{65}$$

The finite element procedures to determine the p_{IJ}'s are:

For $p_{33}(\omega)$: find $u^{(h,33)} \in \mathcal{W}_{33}^h(\Omega)$ such that

$$\Lambda(u^{(h,33)}, v) = -\langle \Delta P, v \cdot \nu \rangle_{\Gamma^T}, \quad \forall v \in \mathcal{W}_{33}^h(\Omega). \tag{66}$$

For $p_{11}(\omega)$: find $u^{(h,11)} \in \mathcal{W}_{11}^h(\Omega)$ such that

$$\Lambda(u^{(h,11)}, v) = -\langle \Delta P, v \cdot \nu \rangle_{\Gamma^R}, \quad \forall v \in \mathcal{W}_{11}^h(\Omega). \tag{67}$$

For $p_{13}(\omega)$: find $u^{(h,13)} \in \mathcal{W}_{13}^h(\Omega)$ such that

$$\Lambda(u^{(h,13)}, v) = -\langle \Delta P, v \cdot \nu \rangle_{\Gamma^R \cup \Gamma^T}, \quad \forall v \in \mathcal{W}_{13}^h(\Omega). \tag{68}$$

For $p_{55}(\omega)$: find $u^{(h,55)} \in \mathcal{W}_{55}^h(\Omega)$ such that

$$\Lambda(u^{(h,55)}, v) = -\langle g, v \cdot \nu \rangle_{\Gamma \setminus \Gamma^B}, \quad \forall v \in \mathcal{W}_{55}^h(\Omega) \tag{69}$$

For $p_{66}(\omega)$: find $u^{(h,66)} \in \mathcal{W}_{66}^h(\Omega_2)$ such that

$$\Lambda(u^{(h,66)}, v) = -\langle g, v \cdot \nu \rangle_{\Gamma_2 \setminus \Gamma_2^B}, \quad \forall v \in \mathcal{W}_{66}^h(\Omega_2). \tag{70}$$

Uniqueness for the finite element procedures (66)–(70) can be shown with the same argument than for the continuous case. Existence follows from finite dimensionality.

Let us analyze the error associated with the procedure (66). As usual we will employ the approximating properties of the interpolant of the solution $u^{(33)}$ of (39). Let $\mathbf{\Pi}_{h,33}$ be the local bilinear interpolant of $u^{(33)}$ defined on the union of all rectangles $R^{(l)},\ l = 1, \ldots, J^{(f)} + 1$. It is known that $\mathbf{\Pi}_{h,33}$ satisfies the approximating properties

$$\|\varphi - \mathbf{\Pi}_{h,33}\varphi\|_0 + h \sum_{l=1}^{l=J^{(f)}+1} \|\varphi - \mathbf{\Pi}_{h,33}\varphi\|_{1,R^{(l)}} \leqslant Ch^s \|\varphi\|_s, \quad 1 < s \leqslant 3/2. \tag{71}$$

Next we demonstrate the apriori error estimates stated in the following theorem.

Theorem 1. *Let $u^{(33)}$ and $u^{(h,33)}$ be the solutions of (39) and (66), respectively. Assume that the matrices $\mathbf{M}_R(\omega)$ and $\mathbf{M}_I(\omega)$ are positive definite. Also assume that the coefficients $\alpha_R^{(l)}, \alpha_I^{(l)}, \beta_R^{(l)}$ and $\beta_I^{(l)},\ l = 1, \ldots, J^{(f)}$ are positive. Then for sufficiently small $h > 0$ the following error estimate holds:*

$$\begin{aligned}
&\|u^{(33)} - u^{(h,33)}\|_0 + h^{1/2}\left(\sum_{l=1}^{l=J^{(f)}+1} \|u^{(33)} - u^{(h,33)}\|^2_{1,R^{(l)}}\right)^{1/2} \\
&\quad + h^{1/2}\left(\sum_{l=1}^{J^{(f)}} \sum_{j,k} \left[\left\langle [u^{(33)} - u^{(h,33)}]_3, [u^{(33)} - u^{(h,33)}]_3 \right\rangle_{\Gamma_{jk}^{(f,l)}} + \left\langle [u^{(33)} - u^{(h,33)}]_1, [u^{(33)} - u^{(h,33)}]_1 \right\rangle_{\Gamma_{jk}^{(f,l)}}\right]\right)^{1/2} \\
&\leqslant C_{33}(\omega) h \sum_{l=1}^{J^{(f)}+1} \|u^{(33)}\|_{3/2,R^{(l)}}.
\end{aligned} \tag{72}$$

Proof. Set

$$e^{(33)} = u^{(33)} - u^{(h,33)}$$

Subtract (66) from (39) to get the error equation

$$\Lambda(e^{(33)}, v) = 0, \quad \forall v \in \mathcal{W}_{33}^h(\Omega). \tag{73}$$

Choose $v = e^{(33)} + \mathbf{\Pi}_{h,33}u^{(33)} - u^{(33)}$ in (73), take the imaginary part in the resulting equation to get

$$\begin{aligned}
&\sum_{l=1}^{l=J^{(f)}+1} \left(\mathbf{M}_I(\omega)\tilde{\epsilon}(e^{(33)}), \tilde{\epsilon}(e^{(33)})\right)_{R^{(l)}} \\
&\quad + \omega \sum_{l=1}^{J^{(f)}} \sum_{j,k} \left[\left\langle \alpha_I^{(l)} [e^{(33)}]_3, [e^{(33)}]_3 \right\rangle_{\Gamma_{jk}^{(f,l)}} + \left\langle \beta_I^{(l)} [e^{(33)}]_1, [e^{(33)}]_1 \right\rangle_{\Gamma_{jk}^{(f,l)}}\right] \\
&= \mathrm{Im}\left(\Lambda(e^{(33)}, e^{(33)})\right) = \mathrm{Im}\left(\Lambda(e^{(33)}, u^{(33)} - \mathbf{\Pi}_{h,33}u^{(33)})\right) \\
&\leqslant \left|\left(\Lambda(e^{(33)}, u^{(33)} - \mathbf{\Pi}_{h,33}u^{(33)})\right)\right| \leqslant \left|\omega^2(\rho e^{(33)}, u^{(33)} - \mathbf{\Pi}_{h,33}u^{(33)})\right| \\
&\quad + \left|\sum_{l=1}^{l=J^{(f)}+1} \left(\mathbf{M}(\omega)\tilde{\epsilon}(e^{(33)}), \tilde{\epsilon}(u^{(33)} - \mathbf{\Pi}_{h,33}u^{(33)})\right)_{R^{(l)}}\right| \\
&\quad + \left|\sum_{l=1}^{J^{(f)}} \sum_{j,k} \left[\left\langle \alpha^{(l)} [e^{(33)}]_3, [u^{(33)} - \mathbf{\Pi}_{h,33}u^{(33)}]_3 \right\rangle + \left\langle \beta^{(l)} [e^{(33)}]_1, [u^{(33)} - \mathbf{\Pi}_{h,33}u^{(33)}]_1 \right\rangle_{\Gamma_{jk}^{(f,l)}}\right]\right| \equiv |T_1| + |T_2| + |T_3|.
\end{aligned} \tag{74}$$

Let $L_*(A)$ and $L^*(A)$ denote the minimum and maximum eigenvalues of the positive definite matrix A, and set

$$L_{R,*} = L_*(\mathbf{M}_R), \quad L_{I,*} = L_*(\mathbf{M}_I), \quad L^{R,*} = L^*(\mathbf{M}_R), \quad L^{I,*} = L^*(\mathbf{M}_I).$$

Also let

$$\alpha_{n,*} = \min_{\{1 \leqslant l \leqslant J^{(f)}+1\}} \alpha_n^{(l)} \quad \beta_{n,*} = \min_{\{1 \leqslant l \leqslant J^{(f)}+1\}} \beta_n^{(l)}$$
$$\alpha^{n,*} = \max_{\{1 \leqslant l \leqslant J^{(f)}+1\}} \alpha_n^{(l)}, \quad \beta^{n,*} = \max_{\{1 \leqslant l \leqslant J^{(f)}+1\}} \beta_n^{(l)} n = R, I.$$

Then using that $\mathbf{M}_R$ and $\mathbf{M}_I$ are positive definite, from (74) and (57) we conclude that

$$\begin{aligned}
&\frac{C_1 L_{I,*}}{2} \sum_{l=1}^{J^{(f)}+1} \|e^{(33)}\|^2_{1,R^{(l)}} \\
&\quad + \min(\alpha_{I,*}, \beta_{I,*})\, \omega \sum_{l=1}^{J^{(f)}} \sum_{j,k} \left[\left\langle [e^{(33)}]_3, [e^{(33)}]_3 \right\rangle + \left\langle [e^{(33)}]_1, [e^{(33)}]_1 \right\rangle_{\Gamma_{jk}^{(f,l)}}\right] \\
&\leqslant \frac{L_{I,*}}{2} \|e^{(33)}\|^2_{0,\Omega} + |T_1| + |T_2| + |T_3|.
\end{aligned} \tag{75}$$

Let us bound the last three terms in the right hand side of (75). First, if ρ^* denotes the maximum value of the coefficient ρ, using the approximating properties (71) the term T_1 can be bounded as follows:

$$\begin{aligned}|T_1| &\leqslant \omega^2\rho^*\|e^{(33)}\|_0\|u^{(33)} - \mathbf{\Pi}_{h,33}u^{(33)}\|_0\\ &\leqslant \omega^2\rho^*\|e^{(33)}\|_0 h^{3/2}\sum_{l=1}^{J^{(f)}+1}\|u^{(33)}\|_{3/2,R^{(l)}}\\ &\leqslant C_3(\omega)\|e^{(33)}\|_0^2 + C_4 h^3\sum_{l=1}^{J^{(f)}+1}\|u^{(33)}\|^2_{3/2,R^{(l)}}.\end{aligned} \tag{76}$$

Next, using again (71), for δ small to be selected later,

$$\begin{aligned}|T_2| &\leqslant 2\max\left(L^{R,*},L^{I,*}\right)\sum_{l=1}^{J^{(f)}+1}\|e^{(33)}\|^2_{1,R^{(l)}}\|u^{(33)} - \mathbf{\Pi}_{h,33}u^{(33)}\|_{1,R^{(l)}}\\ &\leqslant C_5(\delta)h\sum_{l=1}^{J^{(f)}+1}\|u^{(33)}\|^2_{3/2,R^{(l)}} + \delta\sum_{l=1}^{J^{(f)}+1}\|e^{(33)}\|^2_{1,R^{(l)}}.\end{aligned} \tag{77}$$

Next, note that

$$\begin{aligned}&\left|\left\langle [e^{(33)}]_3, [u^{(33)} - \mathbf{\Pi}_{h,33}u^{(33)}]_3\right\rangle_{\Gamma_{jk}^{(f,l)}}\right|\\ &\leqslant \hat{\delta}\omega\left\langle [e^{(33)}]_3, [e^{(33)}]_3\right\rangle_{\Gamma_{jk}^{(f,l)}}\\ &\quad + C_6(\delta,\omega)\left(\|u_3^{(33)} - \mathbf{\Pi}_{h,33}u_3^{(33)}\|_{0,\Gamma_{jk}^{(f,l)}} + \|u_3^{(33)} - \mathbf{\Pi}_{h,33}u_3^{(33)}\|_{0,\Gamma_{jk}^{(f,l+1)}}\right)\\ &\leqslant \hat{\delta}\omega\left\langle [e^{(33)}]_3, [e^{(33)}]_3\right\rangle_{\Gamma_{jk}^{(f,l)}}\\ &\quad + C_7(\delta,\omega)\left(\|u_3^{(33)} - \mathbf{\Pi}_{h,33}u_3^{(33)}\|_{1,R^{(l)}} + \|u_3^{(33)} - \mathbf{\Pi}_{h,33}u_3^{(33)}\|_{1,R^{(l+1)}}\right)\\ &\leqslant \hat{\delta}\omega\left\langle [e^{(33)}]_3, [e^{(33)}]_3\right\rangle_{\Gamma_{jk}^{(f,l)}}\\ &\quad + C_8(\hat{\delta},\omega)h\left(\|u^{(33)}\|^2_{3/2,R^{(l)}} + \|u^{(33)}\|^2_{3/2,R^{(l+1)}}\right).\end{aligned} \tag{78}$$

Thus, proceeding similarly with the term $\langle [e^{(33)}]_1, [u^{(33)} - \mathbf{\Pi}_{h,33}u^{(33)}]_1\rangle_{\Gamma_{jk}^{(f,l)}}$ in T_3 we conclude that

$$\begin{aligned}|T_3| &\leqslant \delta\omega\sum_{l=1}^{J^{(f)}}\sum_{j,k}\left[\left\langle \beta_l^{(l)}[e^{(33)}]_3, [e^{(33)}]_3\right\rangle_{\Gamma_{jk}^{(f,l)}} + \left\langle \alpha_l^{(l)}[e^{(33)}]_1, [e^{(33)}]_1\right\rangle_{\Gamma_{jk}^{(f,l)}}\right]\\ &\quad + \max\left(|\alpha^{(l)}|,|\beta^{(l)}|\right)C_8(\delta,\omega)h\sum_{l=1}^{J^{(f)}+1}\|u^{(33)}\|^2_{3/2,R^{(l)}}.\end{aligned} \tag{79}$$

Next, use the bounds (76), (77) and (79) in (75) to see that for an appropriate choice of δ the following inequality holds:

$$\begin{aligned}&\sum_{l=1}^{J^{(f)}+1}\|e^{(33)}\|^2_{1,R^{(l)}}\\ &\quad + \sum_{l=1}^{J^{(f)}}\sum_{j,k}\left[\left\langle [e^{(33)}]_3, [e^{(33)}]_3\right\rangle_{\Gamma_{jk}^{(f,l)}} + \left\langle [e^{(33)}]_1, [e^{(33)}]_1\right\rangle_{\Gamma_{jk}^{(f,l)}}\right]\\ &\leqslant C_9(\omega)\left(\|e^{(33)}\|_{0,\Omega} + h\sum_{l=1}^{J^{(f)}+1}\|u^{(33)}\|^2_{3/2,R^{(l)}}\right).\end{aligned} \tag{80}$$

To estimate the term $\|e^{(33)}\|_{0,\Omega}$ in the right-hand side of (80) we will employ a duality argument. Let us consider the solution ψ of the following (adjoint) problem:

$$\begin{aligned}&\omega^2\rho\psi(\mathbf{x},\omega) - \nabla\cdot\sigma^*(\psi) = e^{(33)},\ \ \Omega\\ &\sigma^{(*,t)})\nu_{t,t+1} = \sigma^{(*,t+1)})\nu_{t,t+1}(x_1,x_3)\in\Gamma^{(f,t)},\\ &\qquad\qquad t = 1,\cdots,J^{(f)},\\ &\left(\sigma^{(*,t)})\nu_{t,t+1}\cdot\nu_{t,t+1},\sigma^{(*,t)})\nu_{t,t+1}\cdot\chi_{t,t+1}\right)^T\\ &= \mathbf{D}^*(\omega)\left([\psi]\cdot\nu_{t,t+1},[\psi]\cdot\chi_{t,t+1}\right)^T,(x_1,x_3)\in\Gamma^{(f,t)},\\ &\qquad\qquad t = 1,\cdots,J^{(f)}\\ &\sigma^{(*,t)})\nu_{t,t+1}\cdot\nu_{t,t+1} = 0,\ \ \Gamma^T\\ &\sigma^{(*,t)})\nu_{t,t+1}\cdot\chi_{t,t+1} = 0,\ \ \Gamma,\\ &\psi\cdot\nu = 0,\Gamma\setminus\Gamma^T.\end{aligned} \tag{81}$$

Here σ^* is defined as in (1) but using the complex conjugates of the coefficients p_{jklm}.

It will be assumed that the solution of problem (81) satisfies the regularity assumption

$$\sum_{l=1}^{J^{(f)}+1}\|\psi\|_{3/2,R^{(l)}} \leqslant C_{10}\|e^{(33)}\|_{0,\Omega}. \tag{82}$$

Testing (81) against $v\in\mathcal{W}_{33}(\Omega)$ we have that

$$\Lambda(v,\psi) = (v,e^{(33)}),\quad v\in\mathcal{W}_{13}(\Omega). \tag{83}$$

Choose $v = e^{(33)}$ in (83) and use (73) to get

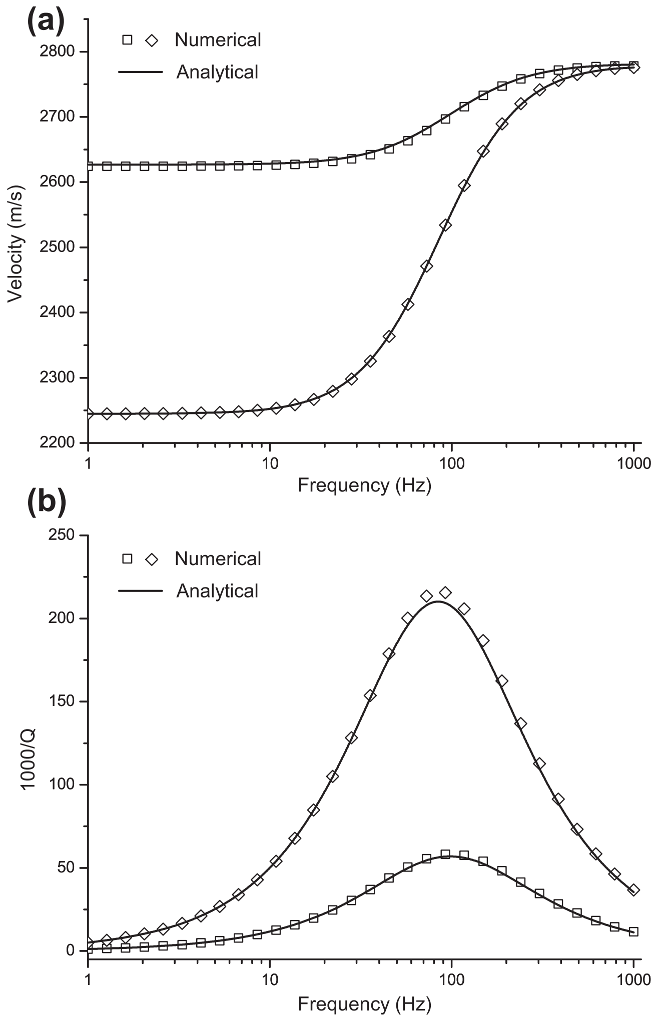

Fig. 2. P-wave phase velocity (a) and dissipation factor (b) as a function of frequency in the direction parallel (squares) and normal (diamonds) to the fractures. The solid lines indicate the theoretical values.

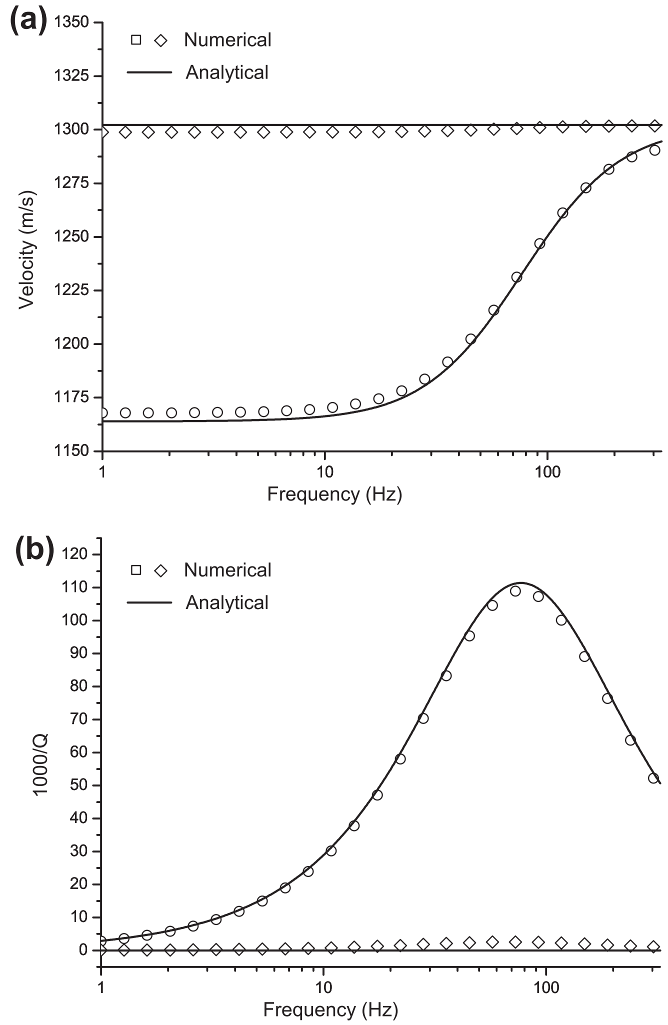

Fig. 3. Phase velocities (a) and dissipation factors (b) as a function of frequency of the quasi-shear vertically polarized wave (qSV-wave, circles) and horizontally polarized (SH-wave, diamonds). The solid lines indicate the theoretical values.

$$
\begin{aligned}
\|e^{(33)}\|_0^2 &= \Lambda(e^{(33)},\psi) = \Lambda(e^{(33)},\psi-\mathbf{\Pi}_{h,33}\psi) = -\omega^2\left(\rho e^{(33)},\psi-\mathbf{\Pi}_{h,33}\psi\right)\\
&+\sum_{l=1}^{J^{(f)}+1}\left(\mathbf{M}(\omega)\tilde{\epsilon}(e^{(33)}),\tilde{\epsilon}(\psi)-\mathbf{\Pi}_{h,33}\psi)\right)_{R^{(l)}}\\
&+\sum_{l=1}^{J^{(f)}}\sum_{j,k}\Bigg[\omega\left\langle\alpha^{(l)}[e^{(33)}]_3,[\psi-\mathbf{\Pi}_{h,33}\psi]_3\right\rangle\\
&+\omega\left\langle\beta^{(l)}[e^{(33)}]_1,[\psi-\mathbf{\Pi}_{h,33}\psi]_1\right\rangle_{\Gamma_{jk}^{(f,l)}}\Bigg]
\end{aligned}
\tag{84}
$$

Next, applying in thee right-hand side of (84) the arguments used to bound the terms T_1, T_2 and T_3 in (74) we get the inequality

$$
\|e^{(33)}\|_0^2 \leqslant \omega^2\rho^* h^{3/2}\|e^{(33)}\|_0^2 + C_{11}\sum_{l=1}^{l=J^{(f)}+1} h^{1/2}\|e^{(33)}\|_0\|e^{(33)}\|_{1,R^{(l)}}^2, \tag{85}
$$

so that for h sufficiently small

$$
\|e^{(33)}\|_0 \leqslant C_{12}h^{1/2}\sum_{l=1}^{J^{(f)}+1}\|e^{(33)}\|_{1,R^{(l)}}. \tag{86}
$$

Thus, using (86) in (80) we see that for h small,

$$
\begin{aligned}
&\sum_{l=1}^{J^{(f)}+1}\|e^{(33)}\|_{1,R^{(l)}}^2\\
&+\sum_{l=1}^{J^{(f)}}\sum_{j,k}\left[\left\langle[e^{(33)}]_3,[e^{(33)}]_3\right\rangle_{\Gamma_{jk}^{(f,l)}}+\left\langle[e^{(33)}]_1,[e^{(33)}]_1\right\rangle_{\Gamma_{jk}^{(f,l)}}\right]\\
&\leqslant C_{13}h\sum_{l=1}^{l=J^{(f)}+1}\|u^{(33)}\|_{3/2,R^{(l)}}^2.
\end{aligned}
\tag{87}
$$

Finally, using (87) in (86) we see that

$$
\|e^{(33)}\|_0 \leqslant C_{14}h\left(\sum_{l=1}^{l=J^{(f)}+1}\|u^{(33)}\|_{3/2,R^{(l)}}^2\right)^{1/2}. \tag{88}
$$

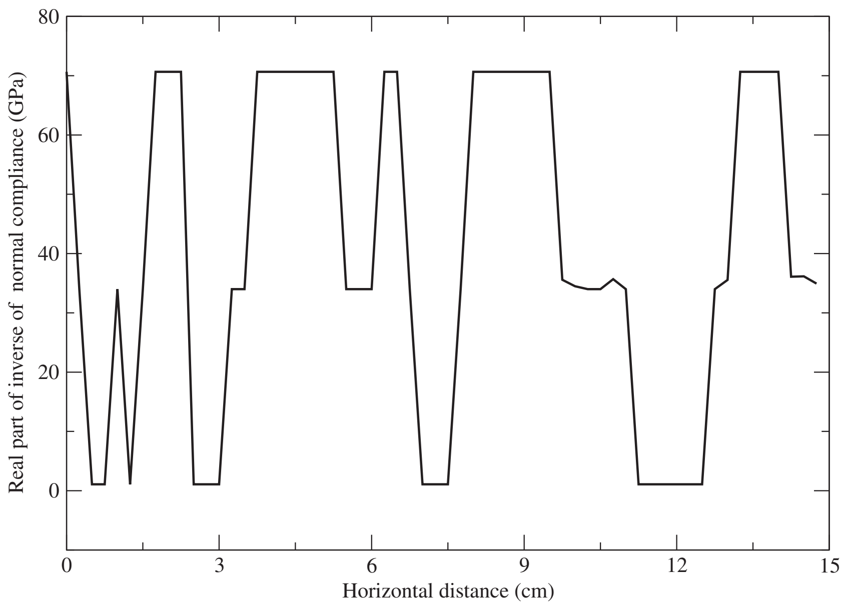

Fig. 4. A 1D restriction of the ternary fractal used to assign values to $L\kappa_N = \mathrm{Re}(Z_N^{-1})$.

Collecting the estimates in (87) and (88) we conclude the validity of the estimate in (72). This completes the proof. $\square$

Remark. An identical argument shows the validity of the error estimate given in Theorem 1 for the solution of the problems (67) and (68).

To analyze the error associated with (69) we use a similar argument to that used to estimate the error associated to the approximate solution of $u^{(33)}$ and the fact that the solution $u^{(55)}$ vanishes on a subset of positive measure of Γ. The analysis is performed in the following theorem.

Theorem 2. *Let $u^{(55)}$ and $u^{(h,55)}$ be the solutions of (42) and (69), respectively. Assume that the matrices $\mathbf{M}_R(\omega)$ and $\mathbf{M}_I(\omega)$ are positive definite and that the coefficients $\alpha_R^{(l)}, \alpha_I^{(l)}, \beta_R^{(l)}$ and $\beta_I^{(l)}$, $l = 1, \ldots, J^{(f)}$ are positive. Then for sufficiently small $h > 0$ the following error estimate holds:*

$$\|u^{(33)} - u^{(h,33)}\|_0 + h^{1/2}\left(\sum_{l=1}^{l=J^{(f)}+1}\|u^{(33)} - u^{(h,33)}\|^2_{1,R^{(l)}}\right)^{1/2} + h^{1/2}\left(\sum_{l=1}^{J^{(f)}}\sum_{j,k}\left[\left\langle[u^{(33)} - u^{(h,33)}]_3, [u^{(33)} - u^{(h,33)}]_3\right\rangle_{\Gamma_{jk}^{(f,l)}} + \left\langle[u^{(33)} - u^{(h,33)}]_1, [u^{(33)} - u^{(h,33)}]_1\right\rangle_{\Gamma_{jk}^{(f,l)}}\right]\right)^{1/2} \leqslant C_{33}(\omega)h\sum_{l=1}^{J^{(f)}+1}\|u^{(33)}\|_{3/2,R^{(l)}}. \tag{89}$$

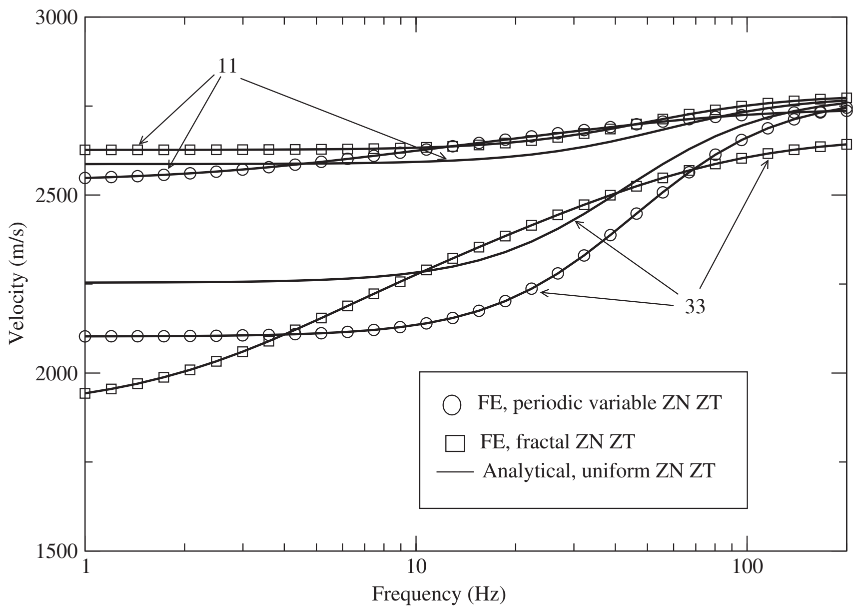

Fig. 5. Phase velocities as a function of frequency in the direction parallel ('11') and normal ('33') to the fractures for variable periodic, fractal and uniform Z_N, Z_T.

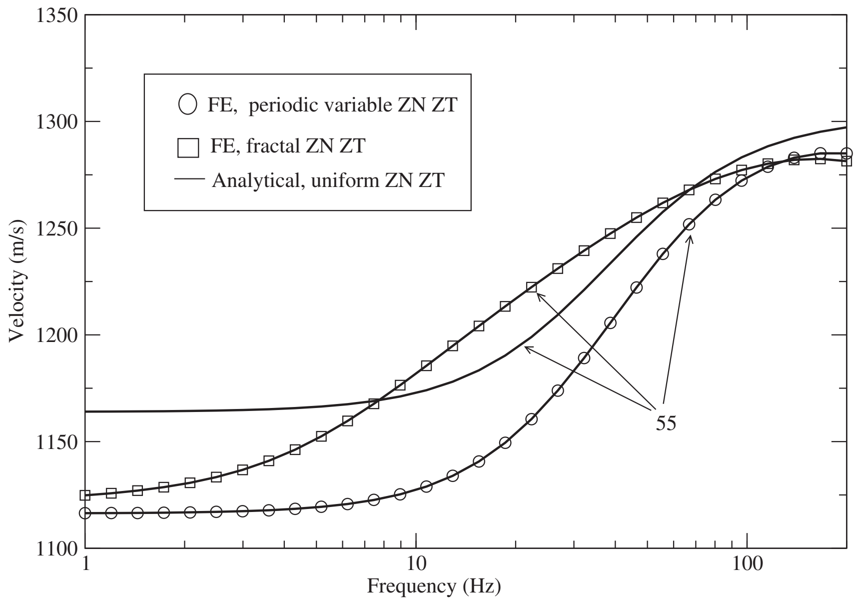

Fig. 6. Phase velocities as a function of frequency of the quasi-shear vertically polarized wave (qSV-wave, label '55') for variable periodic, fractal and uniform Z_N, Z_T.

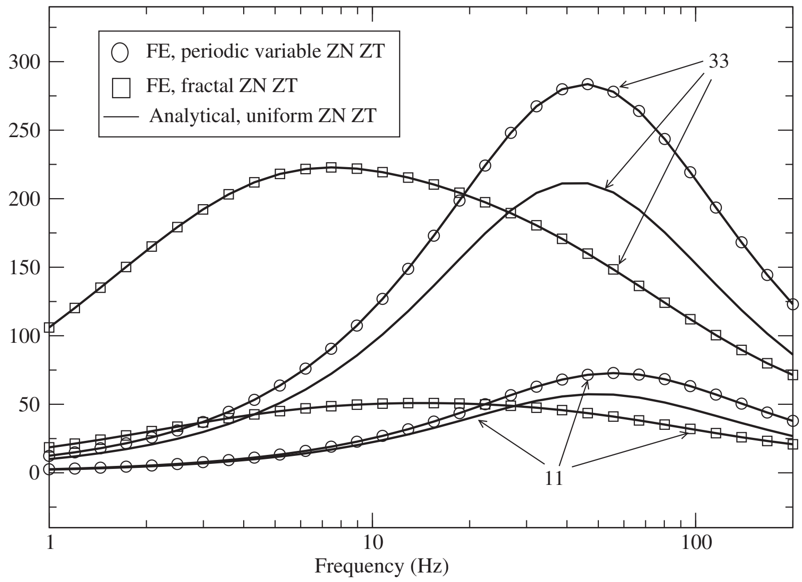

Fig. 7. Dissipation factor as a function of frequency in the direction parallel ('11') and normal ('33') to the fractures for variable periodic, fractal and uniform Z_N, Z_T.

Proof. Let $\mathbf{\Pi}_{h,55}$ be the local bilinear interpolant of $u^{(55)}$ defined on the union of all rectangles $R^{(l)},\ l = 1,\ldots,J^{(f)}+1$. Then $\mathbf{\Pi}_{h,55}$ satisfies the approximating properties

$$\|\varphi - \mathbf{\Pi}_{h,55}\varphi\|_0 + h\sum_{l=1}^{l=J^{(f)}+1}\|\varphi - \mathbf{\Pi}_{h,55}\varphi\|_{1,R^{(l)}} \leqslant Ch^s\|\varphi\|_s, \quad 1 < s \leqslant 3/2. \tag{90}$$

Set

$$e^{(55)} = u^{(55)} - u^{(h,55)},$$

subtract (69) from (42) to get the error equation

$$\Lambda(e^{(55)}, v) = 0, \quad \forall v \in \mathcal{W}^h_{55}(\Omega). \tag{91}$$

Choose $v = e^{(55)} + \mathbf{\Pi}_{h,55}u^{(55)} - u^{(55)}$ in (91), take the imaginary part in the resulting equation, use that $\mathbf{M}_l$ is positive definite, that $\alpha_l^{(l)}$ and $\beta_l^{(l)}$, $l = 1,\ldots,J^{(f)}$ are positive and the fact that $|||\cdot|||_{R^{(l)}}$ defines a norm for $e^{(55)}$ equivalent to the $H^1(R^{(l)})$-norm (see (59)) to get the inequality

$$\begin{aligned}
&\frac{C_2 L_{l,*}}{2}\sum_{l=1}^{J^{(f)}+1}\|e^{(55)}\|^2_{1,R^{(l)}} + \min(\alpha_{l,*},\beta_{l,*})\\
&\quad\times\omega\sum_{l=1}^{J^{(f)}}\sum_{j,k}\left[\left\langle [e^{(55)}]_3, [e^{(55)}]_3\right\rangle_{\Gamma^{(f,l)}_{jk}} + \left\langle [e^{(55)}]_1, [e^{(55)}]_1\right\rangle_{\Gamma^{(f,l)}_{jk}}\right]\\
&\leqslant \left|\omega^2\left(\rho e^{(55)}, u^{(55)} - \mathbf{\Pi}_{h,55}u^{(55)}\right)\right|\\
&\quad+\left|\sum_{l=1}^{l=J^{(f)}+1}\left(\mathbf{M}(\omega)\tilde{\epsilon}(e^{(55)}), \tilde{\epsilon}(u^{(55)} - \mathbf{\Pi}_{h,55}u^{(55)})\right)_{R^{(l)}}\right|\\
&\quad+\left|\sum_{l=1}^{J^{(f)}}\sum_{j,k}\left[\left\langle\alpha^{(l)}[e^{(55)}]_3, [u^{(55)} - \mathbf{\Pi}_{h,55}u^{(55)}]_3\right\rangle\right.\right.\\
&\quad\left.\left.+\left\langle\beta^{(l)}[e^{(55)}]_1, [u^{(55)} - \mathbf{\Pi}_{h,55}u^{(55)}]_1\right\rangle_{\Gamma^{(f,l)}_{jk}}\right]\right| \equiv |T_4| + |T_5| + |T_6|.
\end{aligned} \tag{92}$$

The term T_4 can be bounded as

$$\begin{aligned}
|T_4| &\leqslant \omega^2\rho^*\|e^{(55)}\|_0\|u^{(55)} - \mathbf{\Pi}_{h,55}u^{(55)}\|_0\\
&\leqslant \omega^2\rho^*\|e^{(55)}\|_{0,h^{3/2}}\sum_{l=1}^{J^{(f)}+1}\|u^{(55)}\|_{3/2,R^{(l)}}\\
&\leqslant \delta\sum_{l=1}^{J^{(f)}+1}\|e^{(55)}\|^2_{1,R^{(l)}} + C_4h^3\sum_{l=1}^{J^{(f)}+1}\|u^{(55)}\|^2_{3/2,R^{(l)}}.
\end{aligned} \tag{93}$$

Also, the terms T_5 and T_6 can be bounded as the terms T_2 and T_3 in the proof of Theorem 1 above (cf. (77) and (79)), so that from (92) and (93) we get the estimate

$$\begin{aligned}
&\sum_{l=1}^{J^{(f)}+1}\|e^{(55)}\|^2_{1,R^{(l)}}\\
&\quad+\sum_{l=1}^{J^{(f)}}\sum_{j,k}\left[\left\langle [e^{(55)}]_3, [e^{(55)}]_3\right\rangle_{\Gamma^{(f,l)}_{jk}} + \left\langle [e^{(55)}]_1, [e^{(55)}]_1\right\rangle_{\Gamma^{(f,l)}_{jk}}\right]\\
&\quad\leqslant C_{15}(\omega)h\sum_{l=1}^{J^{(f)}+1}\|u^{(55)}\|^2_{3/2,R^{(l)}}.
\end{aligned} \tag{94}$$

To estimate $\|e^{(55)}\|_0$ we solve again an adjoint problem replacing $e^{(33)}$ by $e^{(55)}$ in (81). A repetition of the argument yields the estimate

$$\|e^{(55)}\|_0 \leqslant C_{16}h^{1/2}\sum_{l=1}^{J^{(f)}+1}\|e^{(55)}\|_{1,R^{(l)}}, \tag{95}$$

and using (94) in (95) we conclude that

$$\|e^{(55)}\|_0 \leqslant C_{17}h\left(\sum_{l=1}^{J^{(f)}+1}\|u^{(55)}\|_{3/2,R^{(l)}}\right)^{1/2}. \tag{96}$$

The validity of Theorem 2 follows from the estimates (94) and (96). This completes the proof. □

6. Numerical results

We developed a proprietary set of codes written in fortran language to implement the finite-element procedures defined and analyzed above. All the numerical tests were run in the SUN workstations at the Department of Mathematics of Purdue University. The discrete boundary value problems to determine the complex stiffnesses p_{IJ} as a function of frequency and the associated phase

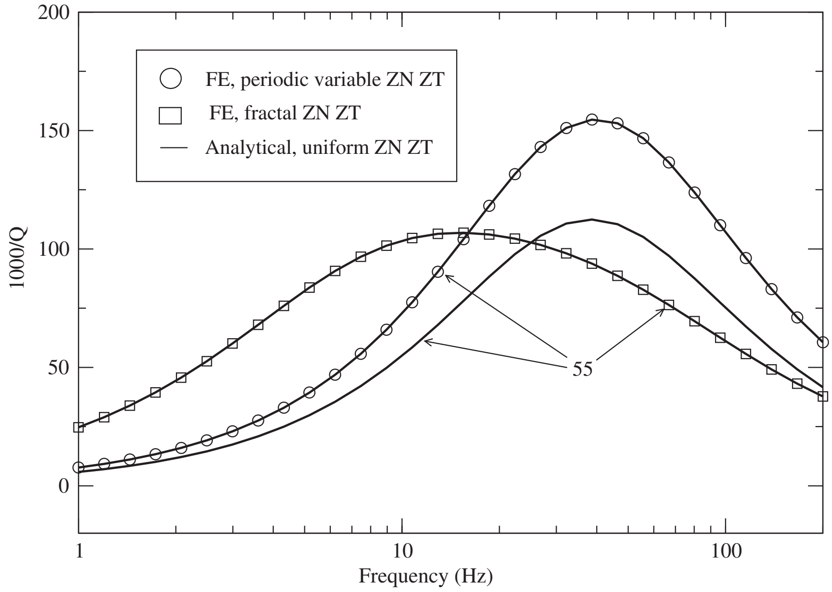

Fig. 8. Dissipation factor as a function of frequency of the quasi-shear vertically polarized wave (qSV-wave, label '55') for variable periodic, fractal and uniform Z_N, Z_T.

Fig. 9. Shear modulus of the fractal shale-limestone composite. Binary fractal of fractal dimension 2.2 and correlation length 0.06 in a scale of 10.

velocities and dissipation coefficients were solved for 30 frequencies in the selected frequency ranges. The associated linear systems of equations were solved using a public domain sparse matrix solver package. This approach yields directly the frequency dependent phase velocities and dissipation coefficients, instead of solving dynamic wave propagation problems in the space–time domain and then using Fourier transforms to obtain the desired frequency domain characterization at the macroscale.

The mesh has a size of 60×60 square elements and represents a square fractured sample of side length 6 cm. The solution of each one of the linear problems associated with the determination of the complex stiffnesses p_{IJ} for a single frequency requires only a few seconds of CPU time in the SUN workstations employed. We consider 29 equally spaced fractures, so the fracture spacing is L = 2 mm. The properties are taken from Chichinina et al. [5] and correspond to experiments on wet fractures (see their Table 1). We consider a background medium defined by λ = 10 GPa, μ = 3.9 GPa and ρ = 2300 kg/m^3. The fractures have the parameters $L\alpha$ = (34 + i 24.9) GPa and $L\beta$ = (15.5 + i 11.24) GPa. The frequency of the signal is f_0 = 50 Hz, at which the long-wavelength approximation is satisfied, since the wavelengths for P and S-waves are about 48 m and 26 m, respectively.

Let us consider, for instance, the normal complex stiffness of the fracture, $L\alpha$. The normal stiffness and viscosity introduced in Eq. (17) can be obtained as κ = 34 GPa/L and η = 24.9 GPa/(2 $\pi f_0 L$). In this manner, a measurement at a given frequency allows us to establish the general frequency dependence in the form of Eq. (17).

The expressions of the wave velocities and quality factors of the different modes are given in Appendix A. Fig. 2 shows the P-wave phase velocity (a) and dissipation factor (b) as function of frequency in the direction parallel (squares and solid lines) and normal (diamonds and solid lines) to the fractures. The solid lines indicate the theoretical values, while symbols indicate the finite element solution. It can be observed a perfect fit of the finite element solution to the theoretical values in the whole frequency range displayed.

Fig. 3 shows the phase velocities (a) and dissipation factors (b) of the quasi-shear vertically polarized wave (qSV-wave, see notation in the appendix) and the horizontally polarized (SH-wave). Again a perfect match between the theoretical and numerical values is observed.

Next we present a collection of simulations for cases in which no analytical solutions are available. In the following examples we employ a mesh of 60 $\times$60 squares elements on a square sample of 15 cm side length and 29 equally spaced fractures, so that the fracture distance is $L = 0.5$ cm.

In the first example we consider two cases of variable complex compliances embedded in a uniform background with properties taken from Chichinina et al. [5] that were used in the previous experiment. In the first case the compliances change periodically taking the values Z_N, Z_T and $2Z_N, 2Z_T$ where Z_N and Z_T have the values of the previous experiment (wet fractures), while in the second case we use a collection of compliances obtained as 1D restrictions of 2D ternary fractals with 100 % variations of the values of Z_N and Z_T used in the previous experiment. The 2D fractals have fractal dimension 2.2 and correlation length 0.3 in a scale of 10. Fig. 4 displays one representative set of values assigned to $\mathrm{Re}(Z_N^{-1}) = L\kappa_N$.

Figs. 5 and 6 display the phase velocities as a function of frequency for these two cases, compared with those of the analytical case for uniform Z_N, Z_T, while Figs. 7 and 8 show the corresponding

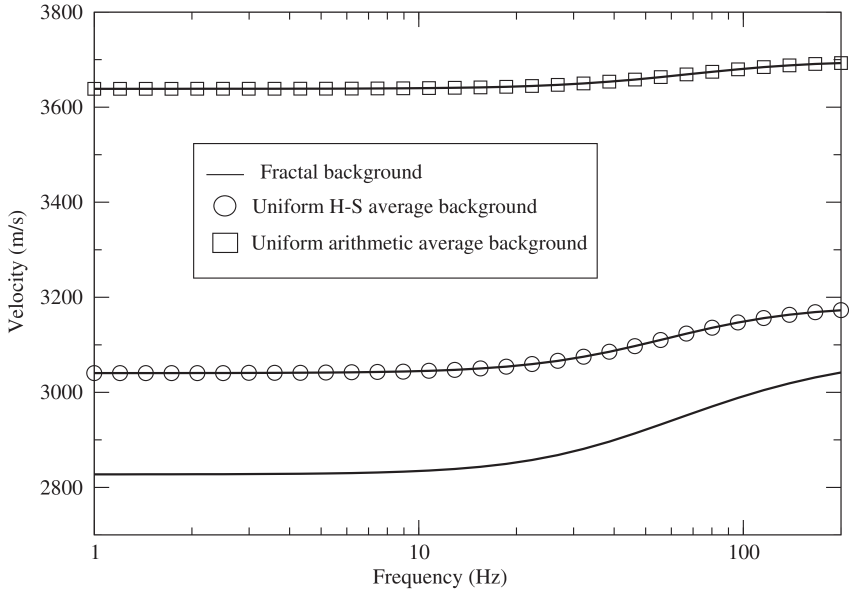

Fig. 10. Phase velocities as a function of frequency in the direction parallel to the fractures when the background is (1) a fractal binary mixture of shale and limestone with 50% shale fraction, (2) uniform chosen as the average of the Hashin–Shtrikman lower and upper bounds of the bulk and shear modulus (H-S label), (3) uniform chosen as the arithmetic averages of the heterogeneous background coefficients.

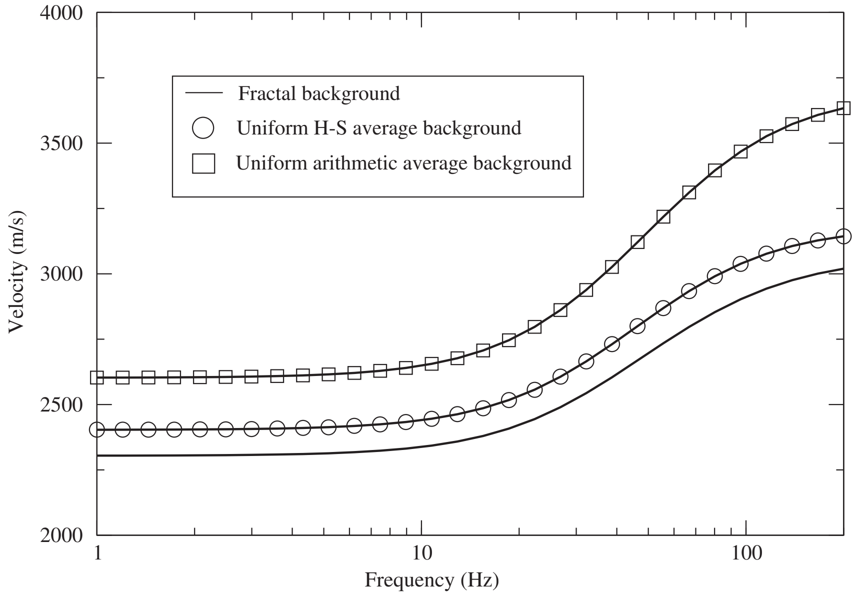

Fig. 11. Phase velocities as a function of frequency in the direction normal to the fractures when the background is (1) a fractal binary mixture of shale and limestone with 50% shale fraction, (2) uniform chosen as the average of the Hashin–Shtrikman lower and upper bounds of the bulk and shear modulus (H-S label), (3) uniform chosen as the arithmetic averages of the heterogeneous background coefficients.

dissipation factors. As expected, in the variable periodic case an increase in fracture compliances is associated with lower phase velocities and higher attenuation for qP waves parallel (labeled '11') and normal (labeled '33') to the fracture plane and qSV waves (labeled '55') as compared with the analytical uniform Z_N, Z_T case. The '33' and '55' waves are the ones having the larger differences with respect to the analytical case. On the other hand, for the fractal Z_N, Z_T case, phase velocities show intermediate values between the analytical and variable periodic cases, with the '33' and '55'' waves showing the larger differences with respect to the analytical curves. An interesting effect is that in the fractal case the attenuation peaks for all the waves shift to low frequencies, with larger differences with respect to the analytical curves of the '11' and '33' waves.

The last example considers the case in which the background is a fractal binary mixture of shale and limestone. The complex compliances Z_N, Z_T are those of the first experiment (wet fractures). The properties of limestone and shale, taken from [15] as follows: limestone has λ = 30 GPa, μ = 25 GPa and ρ = 2700 kg/m^3, while shale has λ = 6.28 GPa, μ = 1.7 GPa and ρ = 2300 kg/m^3. The examples consider 10%, 50% and 90% shale content in the composites. Fig. 9 shows the shear modulus of the highly heterogeneous sample for the case of 50% shale. The coefficients λ and ρ have a similar (correlated) spatial fractal distribution. The fractal dimension is 2.2 and the correlation length is 0.06 (in a scale of 10).

Figs. 10–12 display the phase velocities for the '11', '33' and '55' waves for the case of 50% shale content, while Figs. 13–15 show

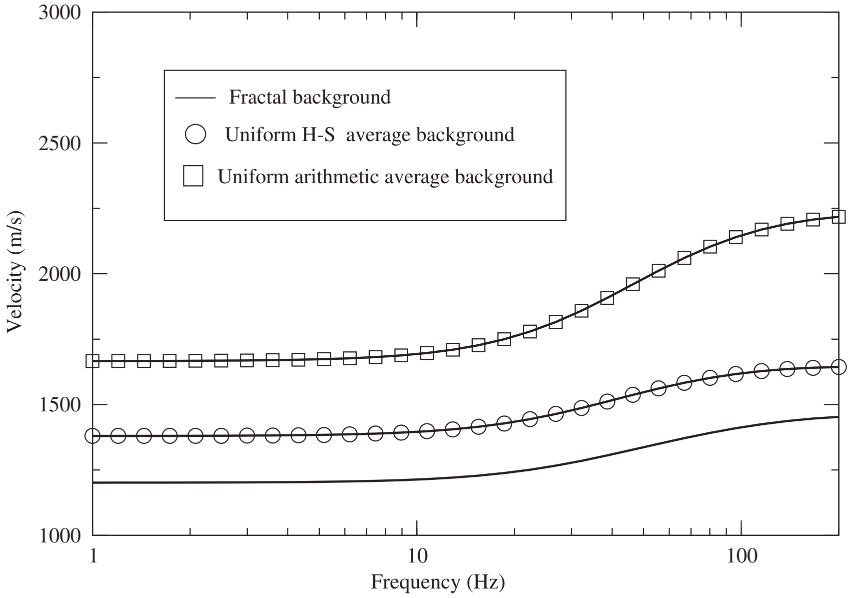

Fig. 12. Phase velocities as a function of frequency for quasi-shear vertically polarized wave (qSV-wave) when the background is (1) a fractal binary mixture of shale and limestone with 50% shale fraction, (2) uniform chosen as the average of the Hashin–Shtrikman lower and upper bounds of the bulk and shear modulus (H-S label), (3) uniform chosen as the arithmetic averages of the heterogeneous background coefficients.

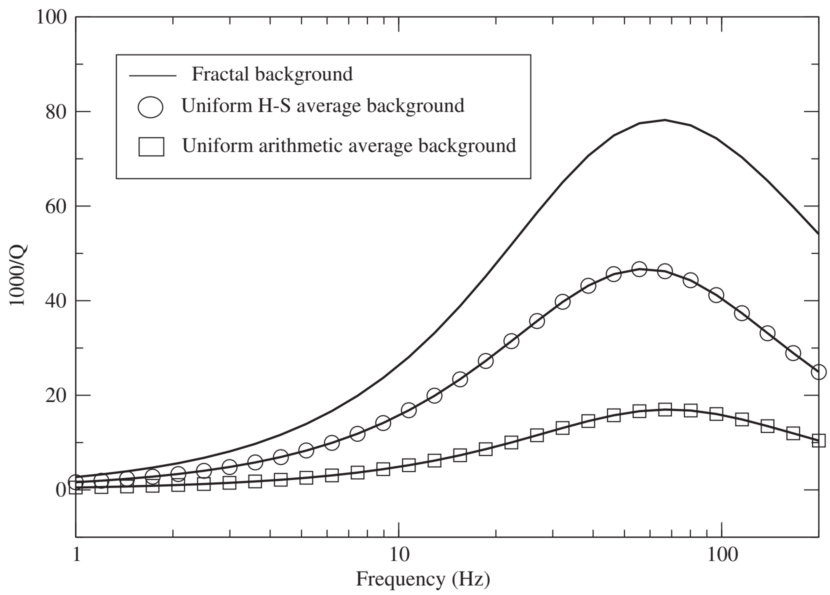

Fig. 13. Dissipation coefficient as a function of frequency in the direction parallel to the fractures when the background is (1) a fractal binary mixture of shale and limestone with 50% shale fraction, (2) uniform chosen as the average of the Hashin–Shtrikman lower and upper bounds of the bulk and shear modulus (H–S label), (3) uniform chosen as the arithmetic averages of the heterogeneous background coefficients.

the corresponding dissipation factors. For reference, these plots also show the curves corresponding to uniform backgrounds constructed using the average of the Hashin–Shtrikman lower and upper bounds of the bulk and shear modulus (curves labeled H-S) and the arithmetic averages of the heterogeneous background coefficients.

It can be observed that the phase velocities for the fractal background case are always lower than the H–S and arithmetic average cases, with the ‘11’ waves being the more affected by the presence of the background heterogeneities. On the other hand, for the ‘11’ waves, the attenuation is much stronger for the fractal background case than for the H–S and arithmetic-average cases. For the ‘33’ and ‘55’ waves, the attenuation is highest for the arithmetic-average case, while Figs. 14 and 15 display curves for fractal and uniform H–S backgrounds showing smaller and almost coincident attenuation up to a peak at about 50 Hz; after 50 Hz the attenuation for the H–S average case decays faster than that of the fractal case.

Finally, Figs. 16 and 17 display the phase velocities and dissipation factors for the ’11’ waves for 10%, 50% and 90% of shale content in the fractal composite. Phase velocities show the expected decrease with decrease in shale content, while dissipation factors exhibit a shift in the attenuation peak as the shale content increases, with maximum attenuation at the intermediate shale content of 50% shale. For brevity, we do not include the corresponding figures for the ‘33’ and ‘55’ waves.

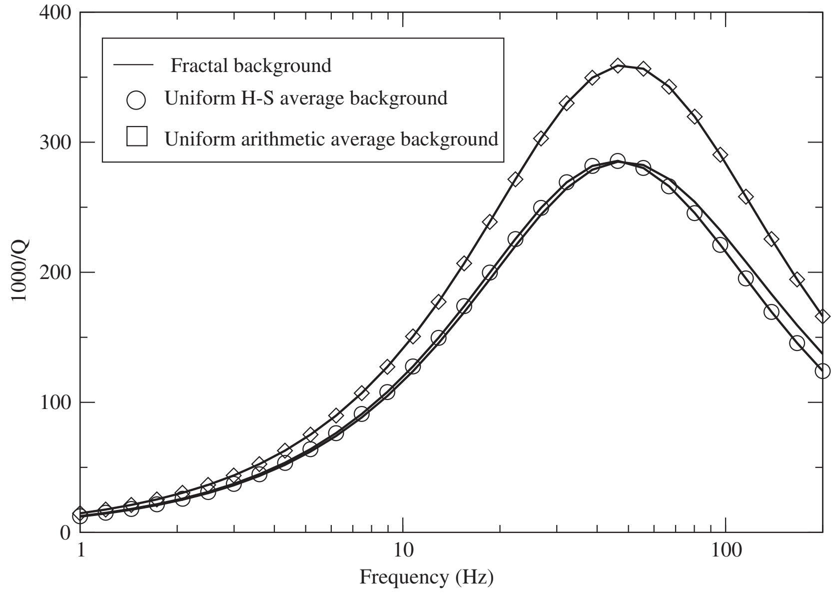

Fig. 14. Dissipation coefficient as a function of frequency in the direction normal to the fractures when the background is (1) a fractal binary mixture of shale and limestone with 50% shale fraction, (2) uniform chosen as the average of the Hashin–Shtrikman lower and upper bounds of the bulk and shear modulus (H–S label), (3) uniform chosen as the arithmetic averages of the heterogeneous background coefficients.

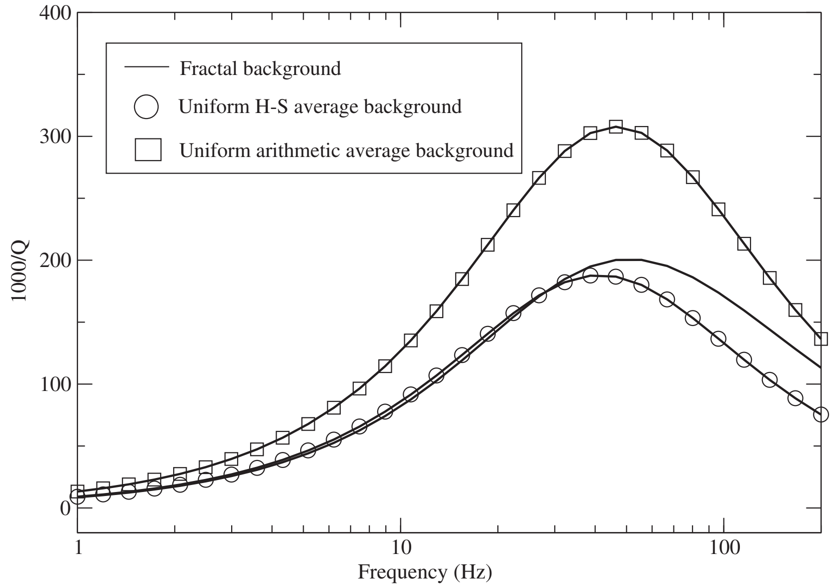

Fig. 15. Dissipation coefficient as a function of frequency for quasi-shear vertically polarized wave (qSV-wave) when the background is (1) a fractal binary mixture of shale and limestone with 50% shale fraction, (2) uniform chosen as the average of the Hashin–Shtrikman lower and upper bounds of the bulk and shear modulus (H–S label), (3) uniform chosen as the arithmetic averages of the heterogeneous background coefficients.

7. Conclusions

Schoenberg's theory predicts that an homogeneous background containing a set of horizontal parallel fractures behaves like a transversely isotropic medium at long wavelengths. We presented a collection of novel numerical quasi-static harmonic experiments to test and validate the theory. The proposed experiments are based on a finite-element solution of the equation of motion for viscoelastic solids in the space-frequency domain to simulate compressibility and shear tests. The fracture behavior is modeled as discontinuities in the displacement and velocity fields and continuity of stresses at the fracture interfaces, i.e., the fractures are represented as a set of internal boundaries in our domain.

We have presented a priori error estimates which are optimal for the regularity of the solution, i.e., we have error on the order of h in the L^2-norm and on the order of $h^{1/2}$ both in the interior broken energy norm and in the L^2-norm on the set of fractures.

For the case of a dense set of equal fractures embedded in an isotropic viscoelastic background, the numerical results show a perfect match with the theoretical values. The advantage of the present methodology is that it can be applied to more general cases for which there are no analytical solutions. To illustrate the capability of the presented methodology to treat more realistic scenarios, we have analyzed the cases of highly heterogeneous backgrounds and variable fracture compliances, for which no

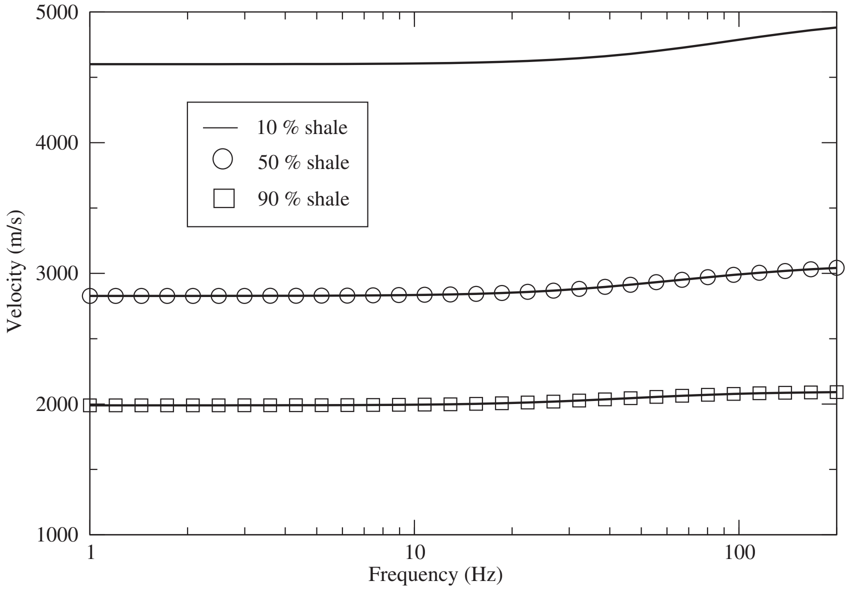

Fig. 16. Phase velocities as a function of frequency in the direction parallel to the fractures when the background is a fractal binary mixture of shale and limestone with 10%, 50% and 90% shale fraction.

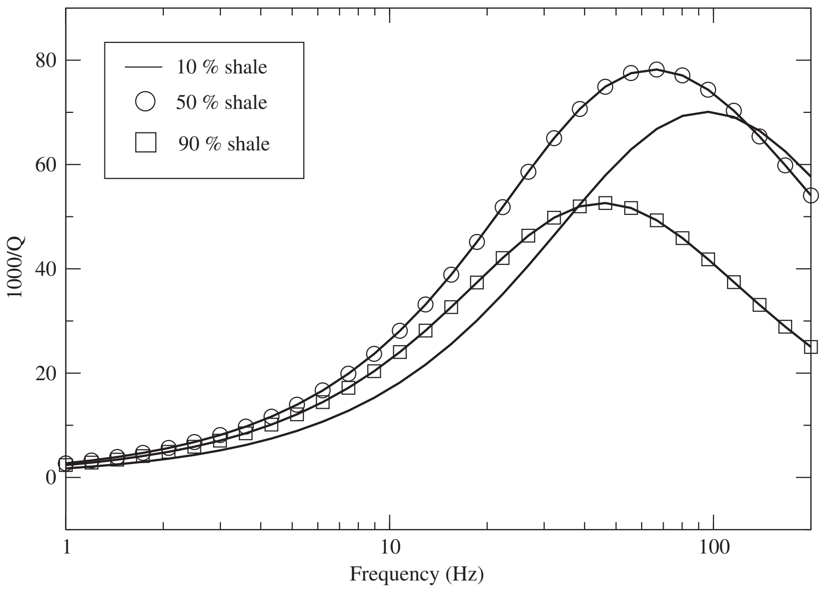

Fig. 17. Dissipation coefficient as a function of frequency in the direction parallel to the fractures when the background is a fractal binary mixture of shale and limestone with 10%, 50% and 90% shale fraction.

equivalent TIV media are available. In both cases, it is concluded that the presence of heterogeneities induce strong changes in the values of the complex stiffnesses of the corresponding effective TIV media. For heterogeneous backgrounds, phase velocities and quality factors for waves parallel to the fracture plane and qSV waves are the ones showing strong departures with respect to the two types of averaged uniform backgrounds used as reference. For variable periodic and fractal complex compliances, phase velocities and dissipation factors of waves parallel and normal to the fracture plane and qSV waves are sensitive to the presence of heterogeneities, with larger differences for waves normal to the fracture plane and qSV waves. Also, in the fractal case attenuation peaks for all waves analyzed shift to lower frequencies.

Acknowledgement

The work of J. E. Santos was partially funded by the GRANT PIP 112-20080100952 from CONICET, Argentina.

Appendix A. Wave velocities and quality factors

The complex velocities are required to calculate wave velocities and quality factors of the fractured medium. They are given by [3]

$$
\begin{aligned}
v_{qP} &= (2\rho)^{-1/2}\sqrt{p_{11}l_1^2 + p_{33}l_3^2 + p_{55} + A} \\
v_{qSV} &= (2\rho)^{-1/2}\sqrt{p_{11}l_1^2 + p_{33}l_3^2 + p_{55} - A} \\
v_{SH} &= \rho^{-1/2}\sqrt{p_{66}l_1^2 + p_{55}l_3^2} \\
A &= \sqrt{[(p_{11} - p_{55})l_1^2 + (p_{55} - p_{33})l_3^2]^2 + 4[(p_{13} + p_{55})l_1 l_3]^2},
\end{aligned}
\tag{A.1}
$$

where $l_1 = \sin\theta$ and $l_3 = \cos\theta$ are the directions cosines, θ is the propagation angle between the wavenumber vector and the symmetry axis, and the three velocities correspond to the qP, qS and SH waves, respectively. The phase velocity is given by

$$
v_p = \left[\mathrm{Re}\left(\frac{1}{v}\right)\right]^{-1}, \tag{A.2}
$$

where v represents either v_{qP}, v_{qSV} or v_{SH}.

The quality factors are given by

$$
Q = \frac{\mathrm{Re}(v^2)}{\mathrm{Im}(v^2)}. \tag{A.3}
$$

References

[1] M. Schoenberg, J. Douma, Elastic wave propagation in media with parallel fractures and aligned cracks, Geophys. Prosp. 36 (1988) 571–590.

[2] J.M. Carcione, Elastodynamics of a non-ideal interface: Application to crack and fracture scattering, J. Geophys. Res. 101 (B12) (1996) 28177–28188.

[3] J.M. Carcione, Wave fields in real media: Wave propagation in anisotropic, anelastic, porous and electromagnetic media, Handbook of Geophysical Exploration, 38, Elsevier, 2007 (2nd edition, revised and extended).

[4] J.M. Carcione, S. Picotti, Reflection and transmission coefficients of a fracture in transversely isotropic media, Stud. Geophys. Geod. 56 (2012). http://dx.doi.org/10.1007/s11200-011-9034-4.

[5] T.I. Chichinina, I.R. Obolentseva, G. Ronquillo-Jarillo, Anisotropy of seismic attenuation in fractured media: theory and ultrasonic experiment, Transp. Porous Media 79 (2009) 1–14.

[6] J.M. Carcione, J.E. Santos, S. Picotti, Fracture-induced anisotropic attenuation, Rock Mech. Rock Eng (2012), http://dx.doi.org/10.1007/s00603-012-0237-y.

[7] M. Schoenberg, K. Helbig, Orthorhombic media: modeling elastic wave behavior in a vertically fractured earth, Geophysics 62 (1997) 1954–1974.

[8] V. Grechka, M. Kachanov, Effective elasticity of rocks with closely spaced and intersecting cracks, Geophysics 71 (3) (2006) D85–D91.

[9] V. Grechka, M. Kachanov, Effective elasticity of fractured rocks: a snapshot of the work in progress, Geophysics 71 (6) (2006) W45–W58.

[10] V. Grechka, Comparison of the non-interaction and differential schemes in predicting the effective elastic properties of fractured media, Int. J. Fract. 144 (2007) 181–188.

[11] E.H. Saenger, O.S. Kruger, S.A. Shapiro, Effective elastic properties of fractured rocks: dynamic vs. static considerations, Int. J. Fract. 139 (2006) 569–576.

[12] E.H. Saenger, R. Ciz, O.S. Kruger, S.M. Schmalholz, B. Gurevich, S.A. Shapiro, Finite-difference modeling of wave propagation on microscale: a snapshot of the work in progress, Geophysics 72 (5) (2007) SM293–SM300.

[13] R. Marrett, S.E. Laubach, J.E. Olson, Anisotropy and beyond: geologic perspectives on geophysical prospecting for natural fractures. The leading edge, vol. 26, 2007, pp. 1106–1111. Reprinted in Fractured reservoirs: a compendium of influential papers 2008, AAPG.

[14] J.E. Santos, J.M. Carcione, S. Picotti, Viscoelastic-stiffness tensor of anisotropic media from oscillatory numerical experiments, Comput. Methods Appl. Mech. Engrg. 200 (2011) 896–904.

[15] J.M. Carcione, Anisotropic Q and velocity dispersion of finely layered media, Geophys. Prospect. 40 (1992) 761–783.

[16] M. Schoenberg, Reflection of elastic waves from periodically stratified media with interfacial slip, Geophys. Prosp. 31 (1983) 265–292.

[17] H. Kolsky, Stress Waves in Solids, Dover publications, New York, 1963.

[18] R.A. Adams, Sobolev Spaces, Academic Press, 1975.

[19] J.M. Carcione, Wave propagation in anisotropic linear viscoelastic media theory and simulated wavefields, Geophys. J. Int. 101 (1990) 739–750. Erratum: 111 (1992) 191.

[20] C.L. Ravazzoli, J.E. Santos, A theory for wave propagation in porous rocks saturated by two-phase fluids under variable pressure conditions, Bollettino di Geofisica teorica ed applicata 46 (2005) 261–285.

[21] B.E.J. Dahlberg, C.E. Kenig, G.C. Verchotta, Boundary value problems for the systems of elastostatics in Lipschitz domains, Duke Math. J. 57 (1988) 795–818.

[22] J.A. Nitsche, On Korn's second inequality, RAIRO 15 (1981) 237–249.

[23] P.G. Ciarlet, The Finite Element Method for Elliptic Problems, North Holland, 1980.